ANNEALING OF DEFORMATION TWINS IN ZINC SINGLE CRYSTALS

Dissertation for the Degree of Ph. D.

MICHIGAN STATE UNIVERSITY
WEI HSIUNG KAO

1975

This is to certify that the

thesis entitled

Annealing of Deformation Twins in

Zinc Single Crystals
presented by

Wei Hsiung Kao

has been accepted towards fulfillment
of the requirements for

Ph.D. degree in Metallurgy

Major professor

Date May 12, 1975

O-7639

ABSTRACT

ANNEALING OF DEFORMATION TWINS IN ZINC SINGLE CRYSTALS

BY

Wei Hsiung Kao

The thermal stability of the $\{10\bar{1}2\}$ $\langle 10\bar{1}\bar{1}\rangle$ type deformation twins in hexagonal close-packed zinc single crystals is investigated. A dislocation model is proposed to explain the receding of the twin tip upon annealing. The interaction between the twinning dislocations at the twin tip is analyzed. The results show that the coherent twin boundary energy γ_t must lie between 1.4 ± 0.4 and 2.8 ± 0.8 ergs/cm^2. The receding process is described as a polygonization process assisted by the tension of the twin interfaces.

The dislocations in the trace left behind by a receding twin observed by other research workers as well as the author are found to polygonize after prolonged annealing and form a wall parallel to the basal plane of the matrix. Attempts were made to identify the dislocations in the trace. The results seem to suggest that their Burgers vector is $\vec{c} + \vec{a}$. Each of them would combine with a $(-\vec{a})$ dislocation to become one with Burgers vector $\vec{c}$ and then polygonize.

The present experimental results also show that small twins are thermally unstable. Twins of sizes smaller than 1.4 microns would disappear completely with no surface tilt remaining. Those twins with

thickness lying between 2 to 35 microns would disappear but the surface tilt would partially remain. The magnitude of the change in the surface tilt is found to be approximately 45 to 50 minutes of arc. The fact that smaller twins less than 1.4 micron thickness can be annealed out completely offers an explanation to the outstanding problem that no recrystallization twins have ever been observed in zinc.

ANNEALING OF DEFORMATION TWINS

IN ZINC SINGLE CRYSTALS

by

Wei Hsiung Kao

A DISSERTATION

Submitted to
Michigan State University
in partial fulfillment of the requirements
for the degree of

DOCTOR OF PHILOSOPHY

Department of Metallurgy, Mechanics and Materials Science

1975

To

My Parents

ACKNOWLEDGMENTS

The author wishes to express his gratitude to Professor C. T. Wei, who suggested the problem and gave valuable guidance throughout the project. He sincerely thanks him also for his encouragement during the course of this study. He is indebted to the other members of his guidance committee, Dr. K. Subramanian, Dr. H. Womochel, and Dr. J. Bass.

Special thanks are due to my wife, Marina, for her understanding, help, and encouragement throughout the course of this study. Without her help this work would not have been finished.

TABLE OF CONTENTS

		Page
LIST OF TABLES		vi
LIST OF FIGURES		vii
I.	INTRODUCTION	1
	1.1 Receding of twins during annealing	2
	1.2 Accommodation region	5
	1.3 Emissary dislocations	6
	1.4 Energy of the twin boundary	7
	1.5 Temperature coefficient of γ_t	9
II.	EXPERIMENTAL PROCEDURE	11
	2.1 Preparation of zinc single crystals	11
	2.2 Introduction of deformation twins	16
	2.3 Heat treatment of the specimens	16
	2.4 Polishing and etching	19
	2.5 Interferometry	19
	2.6 Scanning electron microscopy	19
III.	RESULTS	21
	3.1 Receding of the twin	21
	3.2 Dislocations left behind by receded twins	27
	3.3 Polygonization of dislocations in the traces	27
	3.4 Characteristics of dislocations in the trace	32
	3.5 Scanning electron microscopy	32
	3.6 Interferogram	32
	3.7 Annealing of small twins	43

TABLE OF CONTENTS (Continued)

Page

IV. THEORY AND DISCUSSION 46

4.1 The receding of the twin tip and the twin boundary energy 47

4.1.1 A simplified two-dislocation model 47
4.1.2 Dislocation model of a many-layer twin 55
4.1.3 Change in shape of the twin during annealing . . 72

4.2 Characteristics of dislocations left by the receded twin 73

4.3 Surface tilt left by the receded twins 79

4.4 Polygonization of the dislocations in the trace 83

V. CONCLUSIONS 87

BIBLIOGRAPHY 89

APPENDIX A 92

APPENDIX B 94

APPENDIX C 96

LIST OF TABLES

Page

1. Equilibrium positions of dislocations in the single-slip-band model 97

LIST OF FIGURES

Page

1. Zinc specimen sizes and orientations 12

2. Graphite crucible for crystal growing 13

3. Furnace set-up (schematic) 15

4. A $(1\bar{1}02)[1\bar{1}0\bar{1}]$ twin in two specimens of different orientations 17

5. Furnace set-up for heat treatment 18

6. A $(10\bar{1}2)[10\bar{1}\bar{1}]$ twin was annealed at 200°C for 1 hour. Slightly polished. 100X 22

7. $(1\bar{1}02)[1\bar{1}0\bar{1}]$ twins on the $(10\bar{1}0)$ plane of the specimen. 145X 23
   (a) Freshly introduced twin, not polished 23
   (b) 30 minutes at 200°C, polished 23
   (c) 90 minutes at 200°C, polished 23
   (d) 2 1/2 hours at 200°C, polished 24
   (e) 24 hours at 200°C, polished 24
   (f) 48 hours at 200°C, polished 24

8. The shape of a receding twin tip (schematic) 25

9. $(1\bar{1}02)[1\bar{1}0\bar{1}]$ twins on the $(10\bar{1}0)$ plane. 145X 26
   (a) Fresh twins, not polished 26
   (b) 90 minutes at 200°C, polished 26
   (c) 2 1/2 hours at 200°C, polished 26
   (d) 24 hours at 200°C, polished 26
   (e) 48 hours at 200°C, polished 26

10. A trace of etch pips left by a receded twin; specimen was polished and etched after the annealing. 145X 28

11. A polygonized trace of dislocations. The specimen with a $(10\bar{1}2)[10\bar{1}\bar{1}]$ twin was annealed at 200°C for 24 hours and was then etched. 140X 29

12. Polygonized traces left by the receded twins. 24 hrs. at 200°C, etched. 145X 30

LIST OF FIGURES (Continued) Page

13. Pictures showing the sequence of the polygonization process. 150X 31
(a) 2 hours at 200°C, polished and etched 31
(b) same twin as (a), the twin was polished off first, and then the specimen was annealed for another 12 hours, polished and etched. 31

14. A $(1\bar{1}02)[1\bar{1}0\bar{1}]$ twin after annealing at 200°C for 12 hours, then polished and etched. 150X 33
(a) twin trace on $(10\bar{1}0)$ 33
(b) same trace on $(\bar{1}010)$ 33

15. Twins on $(1\bar{1}00)$ prism plane. Specimen was annealed at 200°C for 2 hours, stress was then applied and specimen was etched. 130X 34
(a) $(01\bar{1}2)[01\bar{1}\bar{1}]$ twins 34
(b) $(0\bar{1}12)[0\bar{1}1\bar{1}]$ twin 34

16. Scanning electron micrographs of the etch pips pattern of a receded twin 35
(a) 2,200X 35
(b) 5,000X 35

17. Scanning electron micrographs of the etch pips pattern of a receded twin. 1,800X 36

18. Scanning electron micrographs of two receded twin tips and the traces left behind. 5,000X 37

19. Scanning electron micrograph of the etch pips pattern of a polygonized trace which was left behind by a receded twin. 2,200X 38

20. A $(1\bar{1}02)[1\bar{1}0\bar{1}]$ twin with a polygonized trace. 200°C, 4 hours and etched 39
(a) Optical microscopy, 150X 39
(b) Scanning electron micrograph, 2,000X 39

21. Scanning electron micrographs of the same twin as in Fig. 20. 2,000X 40
(a) Twin tip 40
(b) Bent trace 40

22. Scanning electron micrograph of the etch pips pattern of a freshly introduced $(1\bar{1}02)[1\bar{1}0\bar{1}]$ twin on the $(10\bar{1}0)$ plane. 1,800X 41

23. (a) A freshly introduced twin on the (0001) surface. 300X . . 42
(b) Interference pattern of the same twin. 300X 42
(c) Interference pattern of the same twin after it was annealed at 200°C for 24 hours 42

LIST OF FIGURES (Continued) Page

24. Same twin as in Fig. 23, but viewed from the $(10\bar{1}0)$. 300X . . 44
(a) Fresh twin, corresponding to Fig. 23(a) 44
(b) After annealing, corresponding to Fig. 23(c), etched . . . 44

25. Small twins on (0001) plane. 350X 45
(a) Before annealing 45
(b) After annealing at 200°C for 10 hours 45

26. Dislocation model of a two-layer twin 48

27. Interaction force between two parallel dislocations in the edge orientation. X-component 52

28. Interaction energy between two parallel dislocations in the edge orientation 54

29. The polygonization process of a two-layer twin 56

30. Dislocation model of a many-layer twin 57

31. Interaction forces between the (m+1) th dislocation and the [99-(m+1)] dislocations in the boundary. X-component 60

32. Interaction forces between the (m+1) th dislocation and the j th dislocation. X-component 64

33. Interaction forces between the (m+1)th dislocation and the m-dislocation wall. X-component 65

34. Burgers vectors in hexagonal close-packed lattice 76

35. Slip systems and twin system in zinc crystal 77

36. Reference twin systems 78

37. The polygonization process of the dislocations in the trace left by a receded twin (schematic) 80

38. Dislocation reactions along the boundary of a $(1\bar{1}02)[1\bar{1}0\bar{1}]$ twin and the matrix crystal 81

39. Polygonization process of the dislocations in the trace (schematic). Plane of the drawing is $(11\bar{2}0)$ 84

40. A twin on $(11\bar{2}0)$ plane (schematic) 95

I. INTRODUCTION

Twinning is one of the two modes by which a crystalline solid can be plastically deformed. The other mode, slip, has been studied extensively. On the other hand, due to the complexity of the twinning process, many of its associated phenomena remain to be explored. Twinning is important since experimental evidence seems to link it with fracture in certain cases.

As defined by Friedel[1], a twin is a "polycrystalline edifice built up of two or more homogeneous portions of the same crystal species in juxtaposition and oriented with respect to each other according to well defined laws." Except for a few rare cases[2], the relationship between two parts of a twinned crystal must have a symmetry so that one part can be brought into coincidence with the other part, or the operation of either (1) reflection in a lattice plane of low indices, or (2) rotation through 60°, 90°, 120° or 180° about a lattice row of low indices. The above description of twinning can be applied to all forms of twins, namely, (1) growth twins, which form during solidification at the solid-liquid interface, (2) annealing twins, which form during recrystallization of a cold-worked material, and (3) deformation twins, which form by a shear process in response to an applied stress. In general, growth and annealing twins have only a secondary effect on the deformation behavior of solids, whereas deformation twinning is an important mechanism of plastic deformation in many crystalline solids.

The problems associated with deformation twinning are usually categorized as:

1. Criteria of the active twinning system in a particular type of crystal.
2. Crystallography of the twinning system.
3. Nucleation mechanism.
4. Growth mechanism.

There is yet another aspect of deformation twinning, the thermal stability of the twins, that is also important for understanding the twinning phenomenon. So far, most of the research work with respect to the twinning has been concentrated on the four categories listed above. The problems associated with annealing of deformation twins remain mostly unsolved. It is, therefore, the purpose of the present work to investigate the behavior of deformation twins in zinc single crystals during annealing.

Zinc crystals are known to twin readily when they are oriented unfavorably for the basal slip system to operate under particular loading conditions. The active twin system in zinc. the $\{10\bar{1}2\}\langle 10\bar{1}\bar{1}\rangle$ system, has a twin shear of $\gamma = 0.139$ determined by its crystallography.

1.1 Receding of twins during annealing

In their study of zinc crystals, Mathewson[3,4] and Phillips[4] found that twins contracted upon annealing. The same phenomenon was also observed in the annealing of twinned iron crystals[5,6,7]. Gindin and Startsev[8] annealed twinned bismuth crystals and found that wedge-shaped twins of 50μ in thickness were not annealed out after many hours at 250°C, but twins of 2μ or less were removed completely. Furthermore, wedge-shaped twins started to vanish at the thin end. Garber[9] studied

twinned sodium nitrate crystals and concluded that annealing at 100°C caused the twins to shorten, and they could be completely lost within 15 minutes at 306°C. The thinner the twins, the sooner they were removed during the annealing.

The receding of the twins happens in almost all the hexagonal close-packed (hcp) crystals and also in some of the body-centered cubic (bcc) crystals. Deformation twins in orthohombic α-uranium were investigated by Cahn[10] and Calais et al[11]. They found that the twins were all less than 10 microns in size. The lengthwise absorption of the twins by the matrix began when the crystals were annealed at 630-650°C for 16 hours. The twins eventually became parallel-sided with blunt tips. Klassen-Neklyudova[12] pointed out that the lens-shaped regions in α-uranium were twins of the second kind with irrational K_1 planes. These twin interfaces straightened out upon annealing in an orientation of lower free energy. It was suggested by Cahn[13] that the contraction of the twin tip was determined by the relative states of strain of the twin and the matrix. If the matrix has less strain energy than the twin has, the twin will contract. The swelling of the twin can occur only when the matrix is further strained by slip after the twin is formed.

Using X-ray diffraction method, Lavrent'yev et al[14] studied annealing of the twins by observing the twin traces on (111) plane of some antimony crystals. Their results showed that annealing of the crystals at 600°C caused the disappearance of those twin layers of 5 to 20μ in size, and restored the monocrystallinity of the specimen. The time needed was less than 5 hours. Churchman[15] pointed out that annealing of twinned titanium single crystals at 800°C would cause the twin lamellae to disappear internally, but the surface step originally

generated by the twin lamellae would remain "unaltered." This scientifically puzzling problem was described by Cahn[13] as "The mystery of the smile without the Cheshire cat." Not all sizes of the disappeared twins would leave behind a surface tilt. Lavrent'yev and Startsev[16] found that upon annealing of zinc crystals at 310°C for 3 hours, most twins disappeared internally and left behind a surface tilt. For those twins whose accommodation regions were smaller than 15μ, both the twin and its accommodation zone would disappear with no surface tilt left behind.

Associated with the surface tilt there is another puzzling phenomenon. Rosebaum[17] found that after the annealing and etching of a zinc single crystal, a partially contracted twin on (0001) cleavage surface might leave behind one or two rows of dislocations in the space previously occupied by the twin lamella. The dislocations can be revealed as etch pits by using a proper etching technique. However, the shear strain produced by the twin was not removed much, if at all. He sugtested that a twin which did not go through the entire crystal would cause a rotation about its composition plane. The amount of rotation would be proportional to the maximum thickness of the twin. Upon annealing, the rotation might remain in the crystal and, if it does, it must be accommodated by a twist boundary of screw dislocations. However, there has been no experimental evidence to substantiate this theory. The characteristics of these dislocations, as well as the mechanism through which they are left by the receding twin, remain to be determined.

Rosenbaum also investigated the possibility of the dislocations at the tip of the twin in zinc being the result of an elastic relaxation. Observations were made of twins on the stage of a microscope both before

and after the bending of the crystal. No evidence of any relaxation was found. Kosevitch and Bashmakov[18] also failed to observe any elastic relaxation of twins in either annealed zinc, antimony, or bismuth crystals. Price[19] used the transmission electron microscopy for studying zinc whiskers and platelets. He noticed that when the beam current was turned on, the twin tip sometimes receded. No dislocations were reported to have been left behind by the receded twin.

1.2 Accommodation region

In zinc crystals, the twin shear causes a change of slope of $3^{o}58'$ of the basal plane, thus making the twin visible in an optical microscope. This twin shear is often accompanied by an accommodation effect which appears on the (0001) surface in the form of a change in the shape of the surface relief around the twin. Since the (0001) slip plane is bent in the accommodation zone during twinning, dislocations of opposite signs form in this plane. Judging from the interference pattern, Lavrent'yev et al[16] have established the fact that the boundary between the accommodation zone and the matrix is convex. It consisted of a wall of the positive parts of dislocation loops. The negative parts of the loops are connected partially with the twin and partially with the slip plane of the accommodation region.

By using interferometry, Moore[20] examined the traces of twins on the cleavage surface of zinc crystals. The traces and the accompanying accommodation kinks were compared with the metallographic sections cut normal to the twin traces. Based on his experimental results, Moore pointed out that the boundary between the accommodation region and the matrix crystal consisted of a number of edge dislocations of the same sign. Lavrent'yev et al[16] made observations of twins in zinc after

successive periods of annealing, X-ray diffraction patterns and interferograms showed that polygonization took place in those twin accommodation regions which were larger than 100 microns. A scheme to account for the observed accommodation pattern was deduced from the results. Direct observation of the polygonization inside the accommodation region of zinc has not been reported.

1.3 Emissary dislocations

Ahead of the advancing tip of a twin there is, in general, a region of stress concentration. In many cases, slip was observed in front of the advancing twin tip[21,22]. Hull[23] studied single crystals of 3.25% silicon iron deformed at 20°K in tension along the <011> axis. He indicated that a twin-matrix boundary of a/6[111] twinning dislocations can be present only when the dislocations are widely spaced, i.e., the twin-matrix boundary is at a very small angle to the twin composition plane. When the twinning dislocation is more closely spaced, the boundary is modified by the occurrence of slip around the end of the twin due to local stress concentration. Sleeswyk[24] proposed the so-called "emissary dislocation" model based on his work with α-iron. He suggested that for a growing twin, where twinning dislocations are piled up behind the advancing tip, every third twinning dislocation -a/6[111] will dissociate into an a/3[111] complementary dislocation and an - a/2[111] emissary dislocation. The emissary dislocation can glide only on the {112} twin composition plane ahead of the twin and produces a homogeneous shear equivalent to the twinning shear without producing a twinned region. The residual incoherent boundary will then consist of - a/6[111] and a/3[111] dislocations and have low energy with no long-range stress. This accounts for the obtuse twin tip angle

in α-iron. No direct experimental evidence to substantiate Sleeswyk's theory has been reported so far.

Cahn[13] theorized that the phenomena associated with receding twins can be explained in terms of Sleeswyk's emissary dislocation model. He indicated that the contraction of a twin lamella becomes possible only when the blunted end becomes an incoherent boundary. This boundary will behave like an ordinary grain boundary, and be able to migrate without concomitant shear. In the case of zinc, Cahn suggested that the twin lamella would emit slip dislocations and then contract. The emitted dislocations would carry the macroscopic shear and could be locked in position by vacancies or tangle with the dislocations in the accommodation region. The thin twins in zinc, which disappear without leaving their shear behind, could be considered to have been removed by the reverse shear due to internal stress.

1.4 Energy of the twin boundary

Twin boundary energy γ_t has been determined for some fcc and bcc metals. The boundary energy can be obtained experimentally through the measurement of the ratio of either γ_t/γ_b or γ_t/γ_s, where γ_b and γ_s represent the grain boundary energy and surface tension, respectively. γ_s is usually measured by the zero-creep method using either thin foils[38] or wires of small diameter[25,26,27]. Fullman[28] obtained γ_t/γ_b in copper by measuring the dihedral angles formed at the intersections of twin boundaries and grain boundaries. The mean value of γ_t/γ_b was found to be 0.035 ± 0.006. Taking γ_b as 600 ergs/cm^2, γ_t of copper is then approximately 21 ergs/cm^2. In a similar attempt[29], γ_t of the incoherent twin boundary energy in copper was found to be 480 ergs/cm^2.

Using interference microscopy, Mykura[31,30] measured the grooves formed at the intersections of annealing twin boundaries and the surfaces of some nickel sheets. The orientation dependence of γ_t was then determined by applying Herring's equation[32]. Kurdman and Cadek[33] applied the same method to sixteen different fcc crystals and alloys for determining the coherent twin boundary energies. The ratios were found to lie between 0.015 and 0.022 with γ_t estimated to lie between 26.8 and 37.6 ergs/cm^2.

Bhandari et al[34] used thermal grooving and interferometric techniques for measuring the interfacial energy of coherent and incoherent deformation twin boundaries in relation to several crystallographic surfaces of some rhombohedral-hexagonal α-aluminum oxide crystals. γ_t/γ_s for the coherent boundary was found to be 0.31 with no significant variation from one sample to another. For the incoherent twin boundary, $\gamma_t/\gamma_s \cong 0.58$ for the $(10\bar{1}0)$ surface plane. By taking 905 ergs/cm^2 as the average value of γ_s of alumina at 1850°C, γ_t was then found to be 282 ergs/cm^2 for the coherent twin boundary energy.

All the values of γ_t mentioned above were obtained by indirect methods. The mean values of γ_s and γ_b were used for computing γ_t at high temperatures. The room temperature γ_t was then obtained by extrapolation from the high temperature values. In such a method, the grain boundary torque in a twin boundary-grain boundary intersection and the variations in the surface tension with crystallographic orientation were assumed either constant or negligible. The errors introduced by these assumptions may be insignificant when γ_t is large, as in alumina, but they may become appreciable in metals with small γ_t.

Thus the values of γ_t so obtained may not always be reliable for some metals.

Nilles and Olson[35] have obtained a relative energy value of 0.081 $\pm$ 0.019 for γ_t/γ_s for the deformation twins in bcc iron crystals. The corresponding coherent twin boundary energy should then be 160 ergs/cm^2. No direct measurements of deformation twin energies are known for hcp metals. Yoo and Wei[36] considered the growth mechanism of twins in zinc single crystals and estimated that γ_t should be 1.4 $\pm$ 0.4 ergs/cm^2.

1.5 Temperature coefficient of γ_t

Murr[37] has shown, from Gibbs fundamental equation, that the temperature coefficient of twin boundary energy of pure metals should be negative. By comparing the values of stacking fault energy γ_{sf} measured indirectly using the zero-creep method with the values measured directly from the extended stacking-fault nodes in an electron microscope of many fcc crystals, it appears that $d\gamma_t/dT$ decreases with γ_t. For instance, in silver, γ_t = 11 ergs/cm^2 and $d\gamma_t/dT$ = -0.003 ergs-cm^{-2}-deg^{-1}. In the case of platinum, γ_t = 161 ergs/cm^2 and $d\gamma_t/dT$ = -0.040 ergs-cm^{-2}-deg^{-1}. McLean et al[38] measured $d\gamma_t/dT$ of cobalt and concluded that its value is small and negative. Kurdman and Cadek[33] also pointed out that the temperature dependence of γ_t was small and hardly measureable for some fcc crystals. Thus, in the case of zinc, the temperature dependence of γ_t may also be negligible.

In the present work an attempt is made to investigate the various phenomena that take place during the annealing of the $(10\bar{1}2)[10\bar{1}\bar{1}]$

deformation twins in zinc crystals, both theoretically and experimentally; namely,

1. The receding of the twins.
2. The energy of the twin interface.
3. Characteristics of the dislocations left behind by a receded twin.
4. The surface tilt associated with a twin before and after annealing.

II. EXPERIMENTAL PROCEDURE

2.1 Preparation of zinc single crystals

Zinc crystals were grown from the melt in a soft mold by using a modified Bridgman technique. The specimen blanks were machined from commercial zinc ingots of 99.99+% purity. The shape and size of the specimen blank is shown in Fig. 1. A single crystal seed with known orientation was then welded to the lower end of the specimen blank with an acetylene torch using ammonium chloride as a flux. Both the specimen blank and the seed were cleaned in diluted hydrochloric acid before and after the welding. Next, the orientation of the seed with respect to the blank was checked by using the back-reflection Laue method. The portion of the blank above the welding joint could be bent when necessary in order to obtain the desired orientation after the crystal-growing operation. The seed end of the specimen was polished for a few minutes in a polishing solution suggested by Vreeland et al[39] to remove the sharp corners at the welding joint and any surface imperfections introduced during handling.

The specimen blank was then placed in a graphite crucible with the seed end of the blank placed in the slot at the top face of the lower thermal block T_1 as shown in Fig. 2. A mixture of fine alumina and graphite powder was then packed around the specimen blank. The slot of the upper thermal block T_2 was placed over the top of the specimen

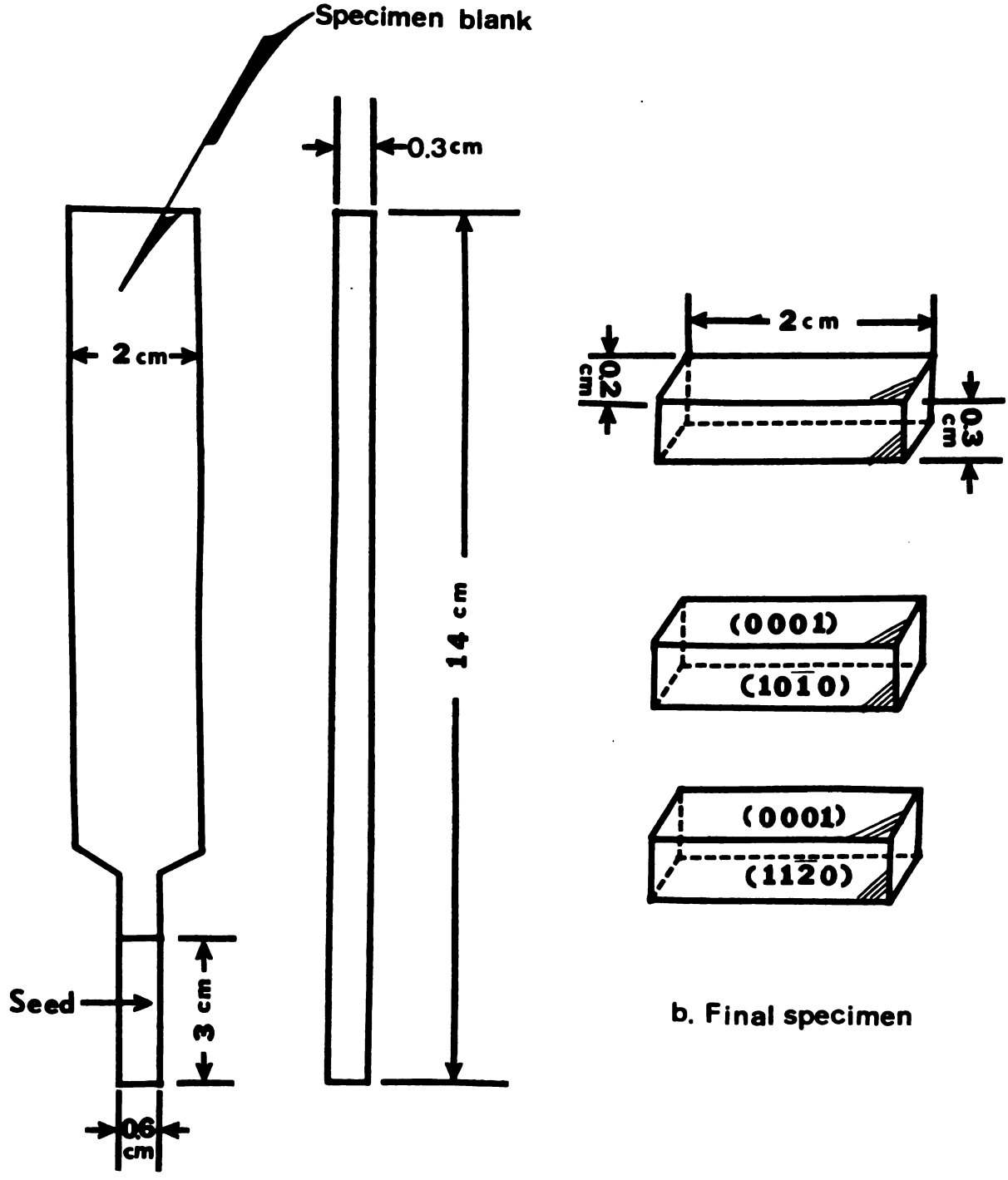

Fig. 1. Zinc specimen sizes and orientations.

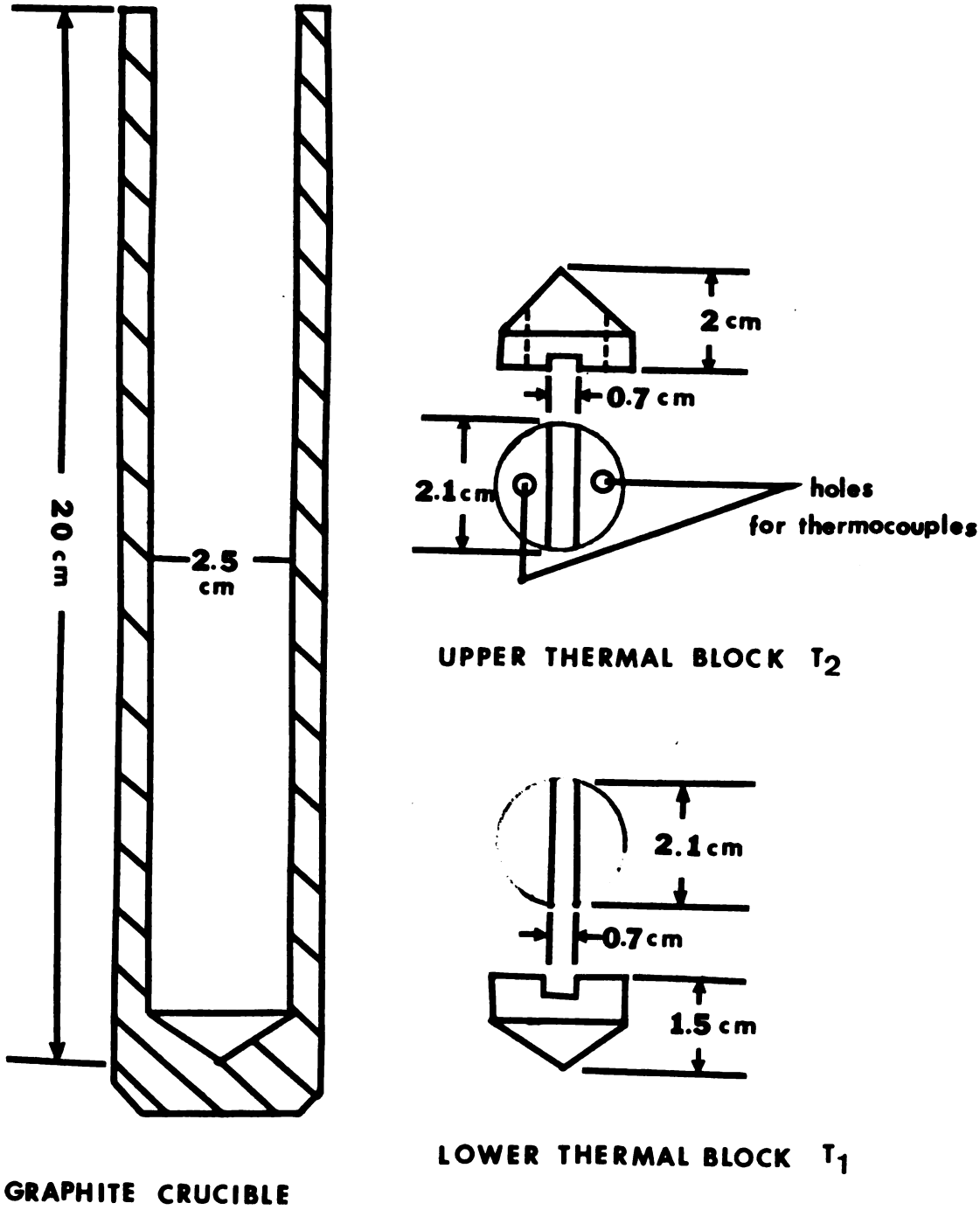

Fig. 2. Graphite crucible for crystal growing.

blank. Two thermocouples were placed inside the crucible, passing through the holes in T_2. One thermocouple was used for monitoring the temperature of the welding junction, the other was positioned 1.5 cm below the junction. This arrangement made it possible to control the position of the solid-liquid interface during the crystal growth.

The crucible was then hung in a furnace, as shown in Fig. 3. After soaking for three hours, and the lowest position of the solid-liquid interface reaching about 1.5 cm below the welding joint, the crucible was slowly lowered through the furnace at the rate of 2.5 cm per hour for growing the crystal in the desired orientation. During the growing process, dry nitrogen or hydrogen flowed through the tube to provide a non-oxidizing atmosphere.

The crystals were grown with either the $<10\bar{1}0>$ or the $<11\bar{2}0>$ direction parallel to the longitudinal axis of the specimen. They were then cleaned in concentrated hydrochloric acid and visually examined. An off-set method[40] was used to eliminate the sub-boundaries, if necessary. The crystal was then checked with the back-reflection Laue method to insure the right orientation. The orientation can also be checked by cleaving the crystal along the basal plane in liquid nitrogen and then examining the orientation of the twin traces on the cleaved plane. The uncertainty in the orientation of the crystals was within $\pm 2^{o}$. Etch pip study showed that the dislocation density in the crystals was approximately 10^{5} cm^{-2}.

The crystals were then cut with a wire saw and cleaved along the basal plane in liquid nitrogen into small pieces of 2 cm x 0.3 cm x 0.2 cm

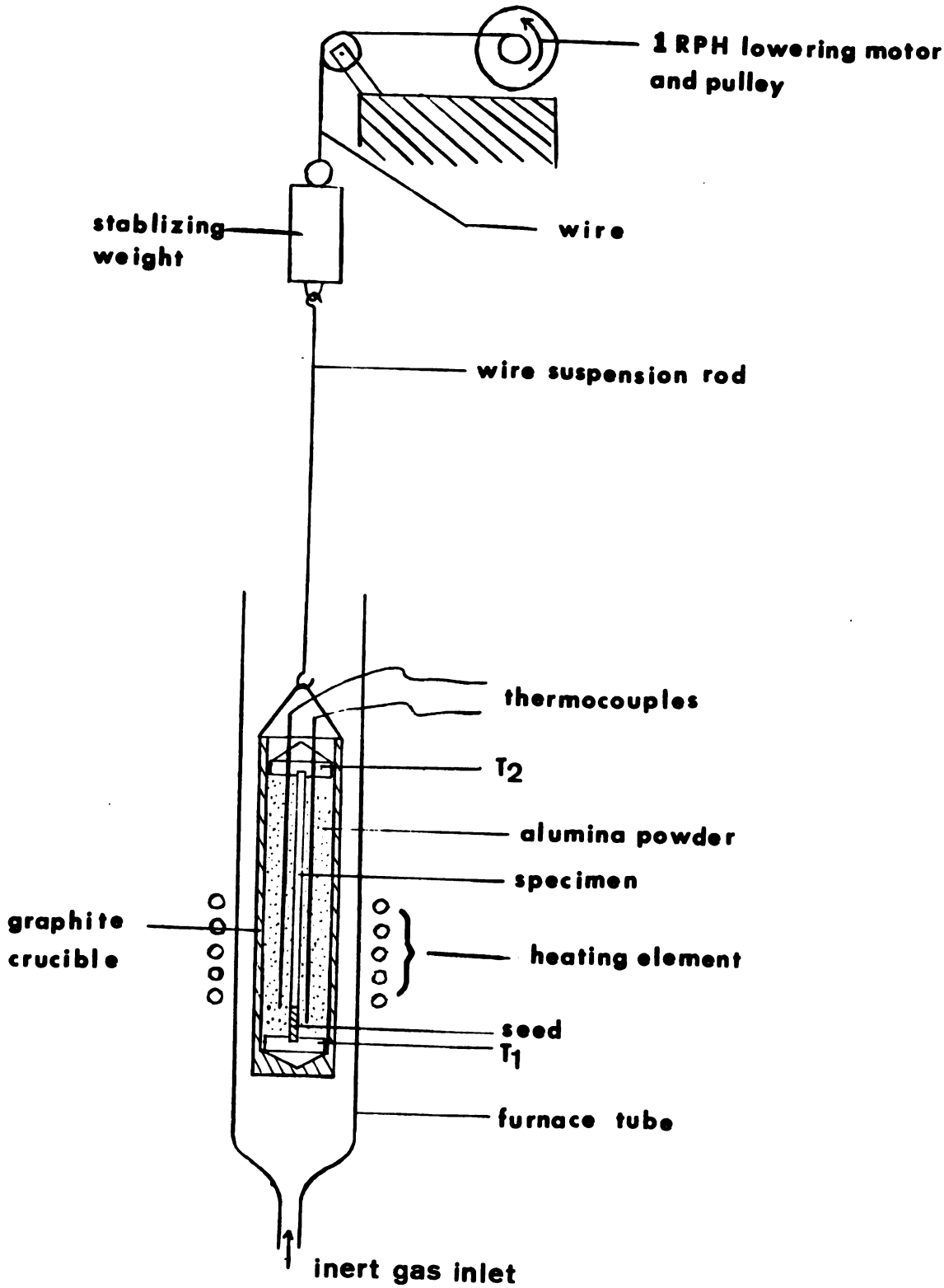

Fig. 3. Furnace set-up (schematic).

in size as shown in Fig. 1. Each piece was chemically polished to remove any surface damage and deformation caused by cutting and cleaving.

2.2 Introduction of deformation twins

Deformation twins were introduced into the zinc crystals either by bending or by point loading applied on the (0001) surface. A twin viewed from the $(11\bar{2}0)$ and $(10\bar{1}0)$ surface respectively is shown in Fig. 4.

In the case of simple bending, the specimen was simply supported on a bending fixture by two knife edges in an Instron testing machine. The load was applied through another knife edge fixed on the crosshead of the testing machine. The knife edges were engaged on the (0001) plane in such a way that either the $\langle 10\bar{1}0\rangle$ or the $\langle 11\bar{2}0\rangle$ direction was parallel to the bending axis.

In the case of point loading, the load was applied on the (0001) surface in the $[000\bar{1}]$ direction by using a pin indenter that was fixed on the crosshead of the Instron machine.

2.3 Heat treatment of the specimens

All the heat treatments were carried out at 200°C. During the heat treatment the specimens were placed in a horizontal tube furnace as shown in Fig. 5. The tube was evacuated first and then a stream of high purity hydrogen was allowed to flow continuously through the tube. The hydrogen was purified by passing through copper turning at 650°C and anhydrous $CaSO_4$. The temperature of the specimen was monitored by a thermocouple in contact with it. The heat-treated specimens were furnace cooled to minimize the thermal stress.

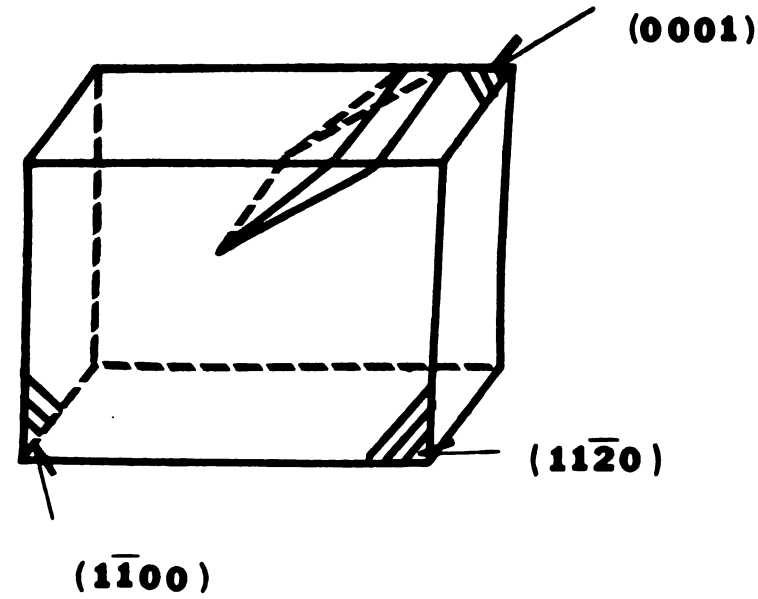

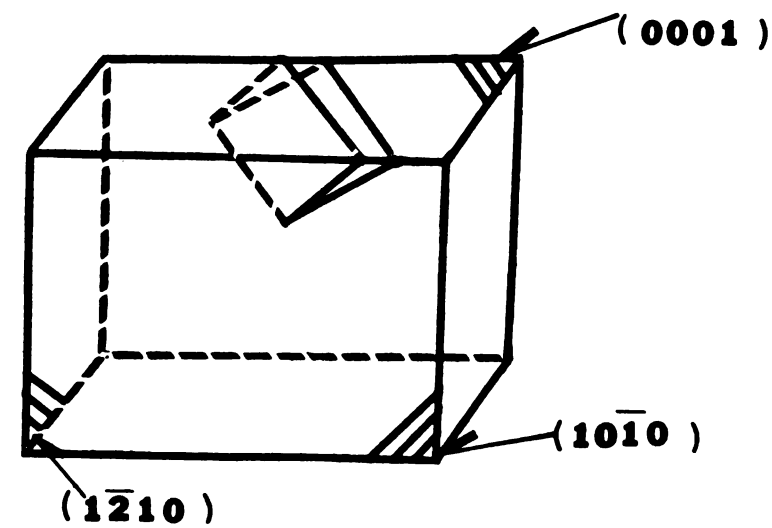

Fig. 4. A $(1\bar{1}02)[1\bar{1}0\bar{1}]$ twin in two specimens of different orientations.

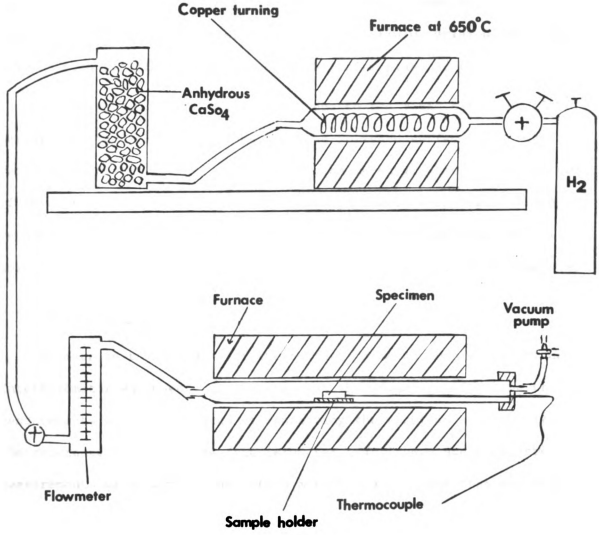

Fig. 5. Furnace set-up for heat treatment.

2.4 Polishing and etching

For polishing and etching undecorated high purity zinc single crystals and revealing the dislocation sites, solutions developed by Vreeland et al[39] (Appendix A) were found to be suitable. The polishing solution could be used successfully on all planes. However, the etching solution could only be used effectively on the $(10\bar{1}0)$ prism plane. Thus all the etch pip studies were made on the prism plane of the specimen.

The formation of the etch pips is due to the rapid diffusion of mercury to the dislocation sites over the polished surface, and the retardation of the rate of polishing by the mercury. During the course of this study, it was found that the etch pips were very difficult to remove from the surface once they were formed. It seems that the P-1 solution can remove them more effectively than P-2 solution (Appendix A).

2.5 Interferometry

To measure the flatness of the surface, a Leitz Double Beam Mirau Interferometer was used. This system has the advantage of making the measurements without the need of contacting the specimen surface with the reference mirror in the interferometer. To insure accuracy, the measurements were carried out with a monochromatic light beam emitted from a sodium vapor lamp.

2.6 Scanning electron microscopy

The topological features of the crystal surface developed by etching were observed with an Advanced Metals Research Scanning Electron Microscope operated at 17 Kv. No coating of the crystal surface was used. The specimens were examined in the emissive mode with a tilting

angle of 41^{o} of the crystal surface with respect to the incident electron beam.

III. RESULTS

3.1 Receding of the twin

In order to observe how the twins might have receded, the specimens were polished slightly after annealing. Both the original position of the twin tip and its position after annealing can be seen in Fig. 6. Further polishing will remove the residual surface tilt left behind by the receded twin tip and only the blunted twin tip will show.

Fig. 7 shows the trace of the twin on the $(10\bar{1}0)$ surface of the specimen after annealing at 200°C for various lengths of time. The specimen was polished heavily after each annealing to remove the residual surface tilt, and then photographed. Fig. 7(f) represents the final shape of the twin tip after 24 hours annealing at 200°C. The final height of the twin tip was found to be within 35×10^{-4} cm. Further annealing did not change the size or shape of the twin. Fig. 8 is a schematic drawing of a receding twin tip.

Fig. 9 shows the change of the twins in a specimen upon annealing at 200°C for various periods of time. It shows that the receding rate of the twin is different from one twin to another and appears to be irregular.

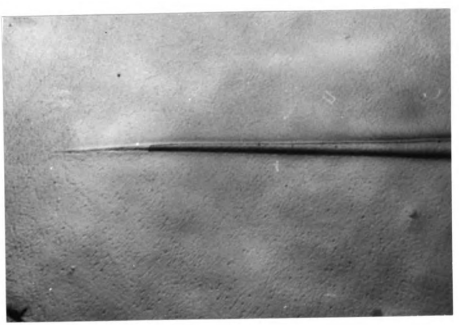

Fig. 6. A $(10\bar{1}2)[10\bar{1}\bar{1}]$ twin was annealed at 200°C for 1 hour. Slightly polished. 100X

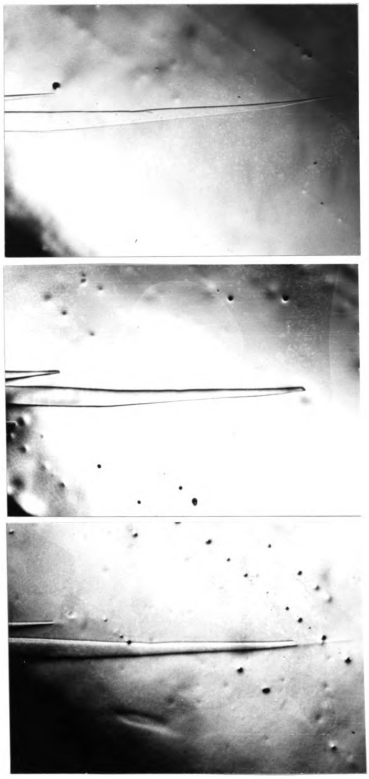

Fig. 7. $(1\bar{1}02)[1\bar{1}0\bar{1}]$ twins on the $(10\bar{1}0)$ plane of the specimen. 145X
(a) Freshly introduced twin, not polished.
(b) 30 minutes at 200°C, polished.
(c) 90 minutes at 200°C, polished.

(d)

(e)

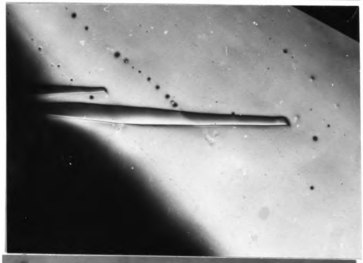

(f)

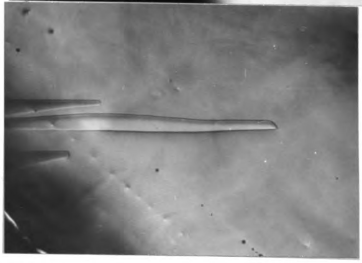

Fig. 7. (Continued) 145X
(d) 2 1/2 hours at 200°C, polished.
(e) 24 hours at 200°C, polished.
(f) 48 hours at 200°C, polished.

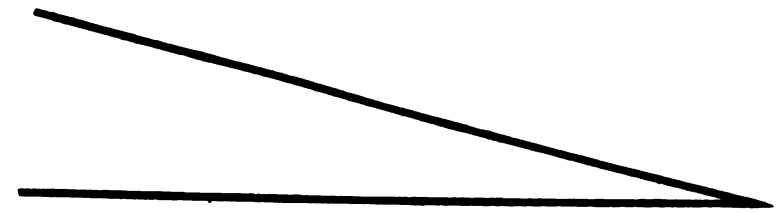

(a)

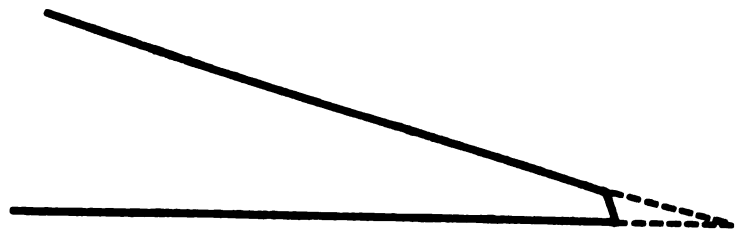

(b)

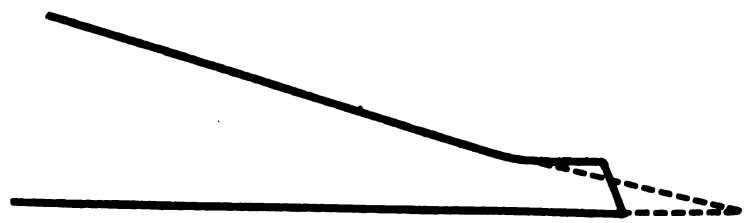

(c)

Fig. 8. The shape of a receding twin tip (schematic).

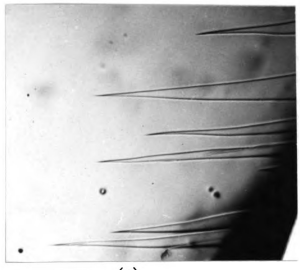

(a)

(b)

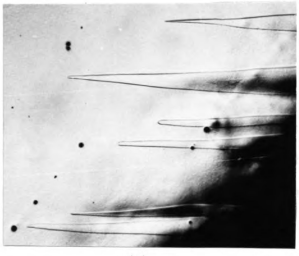

(c)

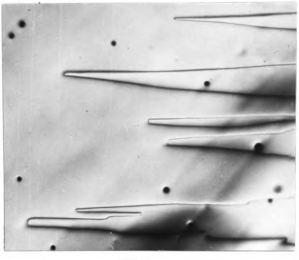

(d)

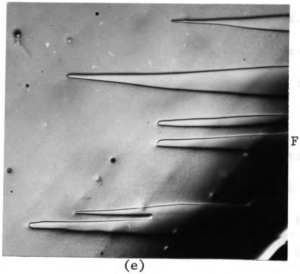

(e)

Fig. 9. $(1\bar{1}02)[1\bar{1}0\bar{1}]$ twins on the $(10\bar{1}0)$ plane. 145X
(a) Fresh twins, not polished.
(b) 90 minutes at 200°C, polished.
(c) 2½ hours at 200°C, polished.
(d) 24 hours at 200°C, polished.
(e) 48 hours at 200°C, polished.

3.2 Dislocations left behind by receded twins

For observing the dislocations left behind by the receded twins, only those twins which extended over the entire thickness of the specimen were selected. It could be assumed that all the twinning dislocations on the twin boundaries in such specimens were of edge character.

Fig. 10 shows the twins after annealing and etching. The etch pips represent the intersecting points of the dislocations with the prism plane. It clearly indicates that a row of dislocations is left behind by the receded twin. The density of the dislocations along the trace was found to be non-uniform.

3.3 Polygonization of dislocations in the traces

In an effort to identify the nature of the dislocations in the traces, a twin introduced by bending was annealed for a prolonged period of time. Fig. 11 shows such a trace of dislocations after annealing at 200°C for 24 hours. The row of dislocations was observed to bend and eventually polygonize. The segment of polygonized dislocation boundary formed at the tip of the row of dislocations was parallel to the trace of the basal plane. Numerous polygonized boundaries of basal dislocations can be seen over the entire specimen. Fig. 12 shows that the polygonization of the dislocations in the trace was stopped when the trace met another boundary.

Fig. 13 shows two intermediate stages of polygonization of the dislocations in the trace. Fig. 13(a) shows the trace after 2 hours of annealing at 200°C. The specimen was then polished to remove all the etch pips and annealed for another 12 hours. The etch-pip pattern of the same specimen after the second annealing is shown in Fig. 13(b).

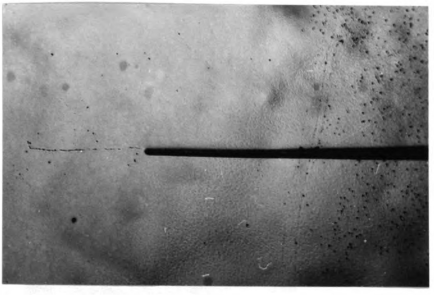

Fig. 10. A trace of etch pips left by a receded twin; specimen was polished and etched after the annealing. 145X.

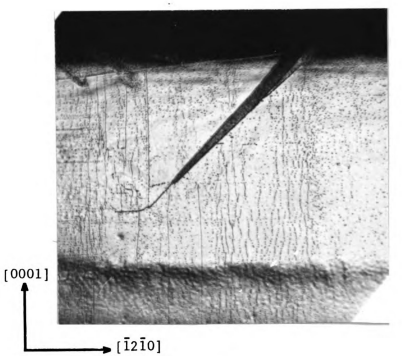

Fig. 11. A polygonized trace of dislocations. The specimen with a $(10\bar{1}2)[10\bar{1}\bar{1}]$ twin was annealed at 200°C for 24 hours and was then etched. 140X

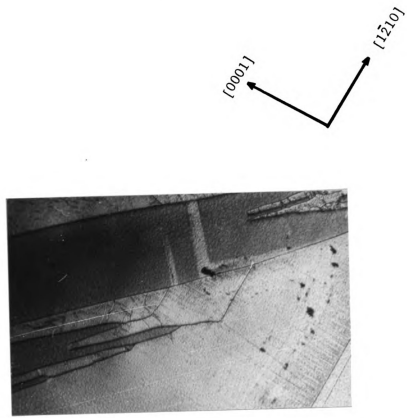

Fig. 12. Polygonized traces left by the receded twins. 24 hrs. at 200°C, etched. 145X

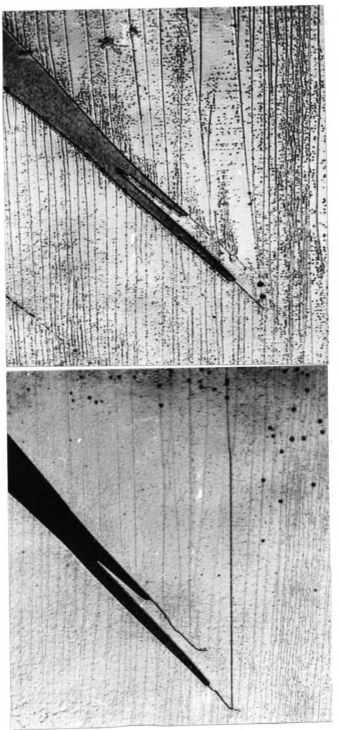

Fig. 13. Pictures showing the sequence of the polygonization process. 150X
(a) 2 hours at 200°C, polished and etched.
(b) same twin as (a), the twin was polished off first, and then the specimen was annealed for another 12 hours, polished and etched.

3.4 Characteristics of dislocations in the trace

Fig. 14 shows the trace of a $(1\bar{1}02)[1\bar{1}0\bar{1}]$ twin on both the front and the back surfaces of the specimen after annealing and etching. These figures appear to be similar.

A specimen with a $(01\bar{1}2)[01\bar{1}\bar{1}]$ twin was annealed at 200°C for 2 hours and pulled in the $[01\bar{1}0]$ direction parallel to its basal plane. Fig. 15 shows the etch-pip pattern on the $(1\bar{1}00)$ plane of the specimen. The applied stress introduced many second-order pyramidal dislocations in front of the receded twin tip. However, the row of dislocations left behind by the receded twin tip were not removed by the applied stress and remained to be a distinctive group. This is an indication that they are not second-order pyramidal dislocations.

3.5 Scanning electron microscopy

Figs. 16 through 19 show the scanning electron micrographs of some receded twin tips after etching. Fig. 20(a) shows an optical micrograph of a twin with a bent trace of etch pips. Fig. 21 is the scanning electron micrographs of the etch pips of the same specimen as in Fig. 20(a) at high magnifications. Fig. 22 is an etch-pip pattern of a freshly formed twin. These micrographs show the detail of the etch pips in the traces and in the twin boundaries.

3.6 Interferogram

The surface tilt of a twin and its change after annealing were examined with the interferometer as described previously. Fig. 23(a) shows a twin and its accommodation zone on the (0001) surface before the

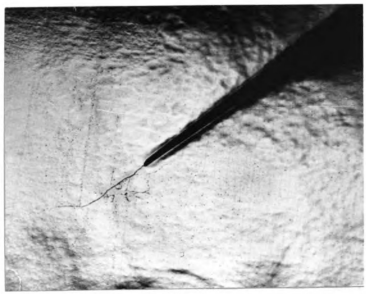

(a)

[0001]

[$1\bar{2}10$]

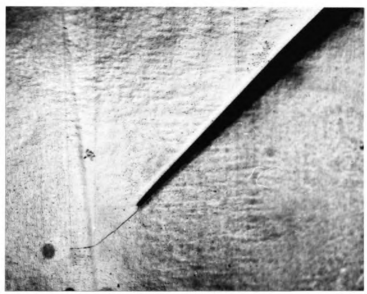

(b)

Fig. 14. A ($1\bar{1}02$)[$1\bar{1}0\bar{1}$] twin after annealing at 200°C for 12 hours, then polished and etched. 150X
(a) twin trace on ($10\bar{1}0$).
(b) same trace on ($\bar{1}010$).

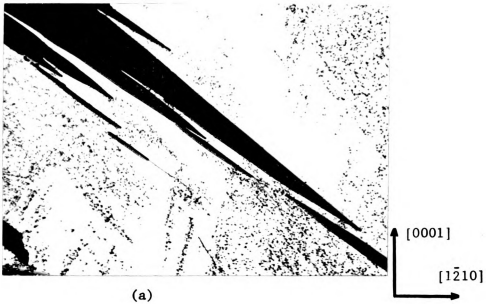

(a)

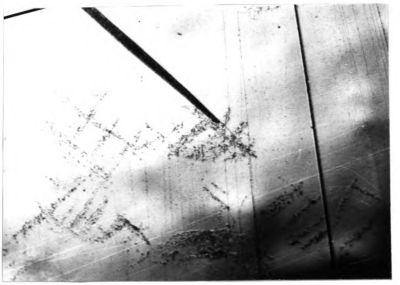

(b)

Fig. 15. Twins on (1$\bar{1}$00) prism plane. Specimen was annealed at 200°C for 2 hours, stress was then applied and specimen was etched. 130X
(a) (01$\bar{1}$2)[01$\bar{1}\bar{1}$] twins.
(b) (0$\bar{1}$12)[0$\bar{1}$1$\bar{1}$] twin.

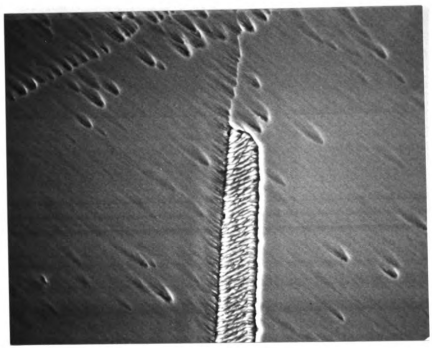

(a)

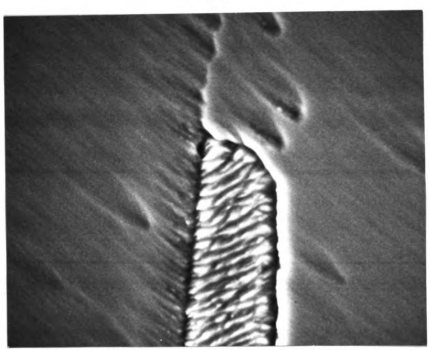

(b)

Fig. 16. Scanning electron micrographs of the etch pips pattern of a receded twin.
(a) 2,200X.
(b) 5,000X.

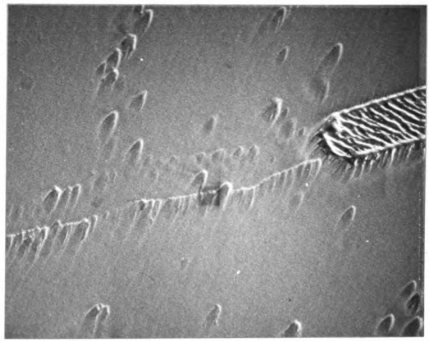

(a)

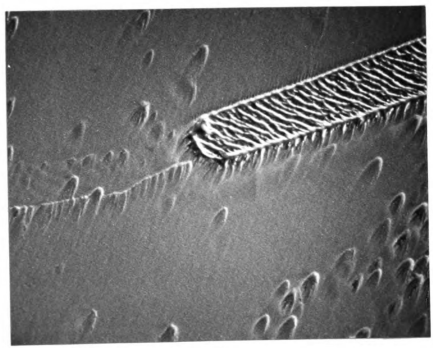

(b)

Fig. 17. Scanning electron micrographs of the etch pips pattern of a receded twin. 1,800X

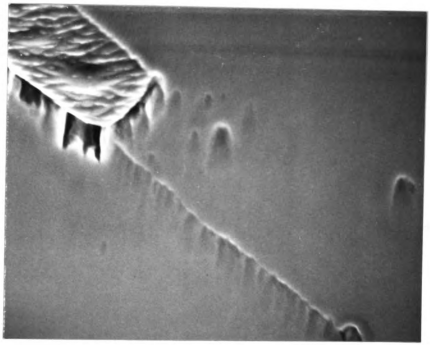

(a)

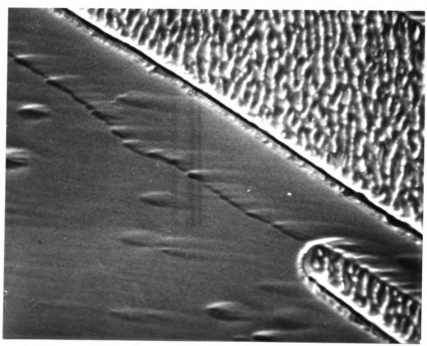

(b)

Fig. 18. Scanning electron micrographs of two receded twin tips and the traces left behind. 5,000X

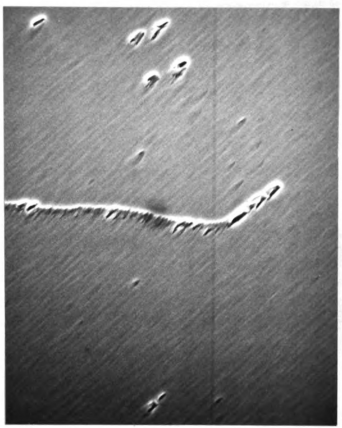

Fig. 19. Scanning electron micrograph of the etch pips pattern of a polygonized trace which was left behind by a receded twin. 2,200X

(a)

(b)

Fig. 20. A $(1\bar{1}02)[1\bar{1}0\bar{1}]$ twin with a polygonized trace. 200°C, 4 hours and etched.
(a) Optical microscopy, 150X
(b) Scanning electron micrograph, 2,000X

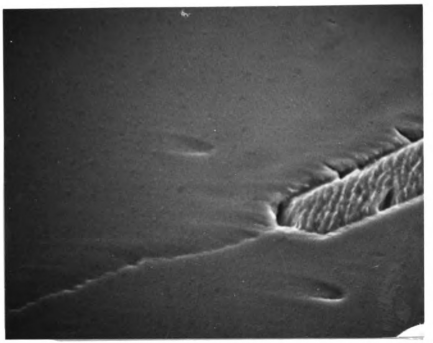

(a)

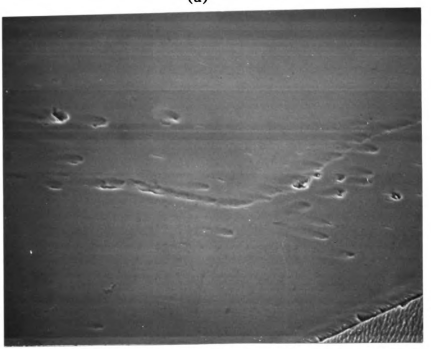

(b)

Fig. 21. Scanning electron micrographs of the same twin as in Fig. 20. 2,000X
(a) Twin tip.
(b) Bent trace.

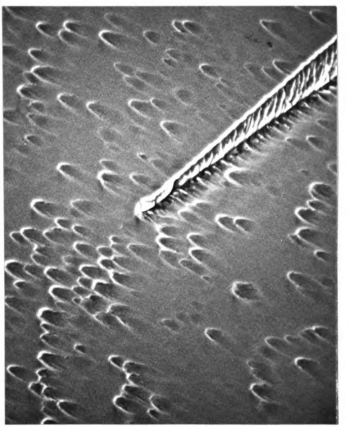

Fig. 22. Scanning electron micrograph of the etch pips pattern of a freshly introduced ($1\bar{1}02$)[$1\bar{1}0\bar{1}$] twin on the ($10\bar{1}0$) plane. 1,800X

(a)

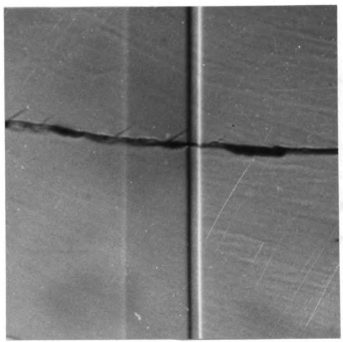

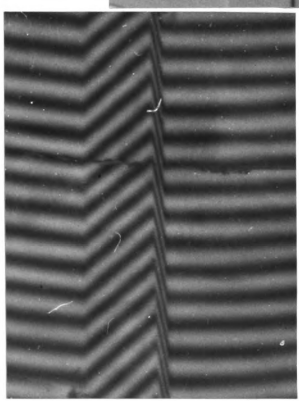

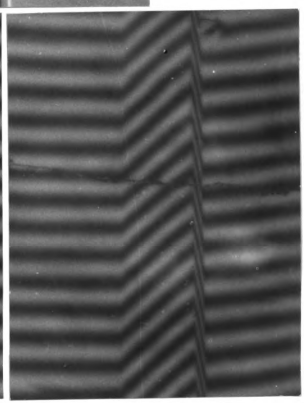

(b) (c)

Fig. 23. (a) A freshly introduced twin on the (0001) surface. 300X
(b) Interference pattern of the same twin. 300X
(c) Interference pattern of the same twin after it was annealed at 200°C for 24 hours.

heat treatment. Fig. 23(b) shows the interference pattern of the same twin. After annealing at 200°C for 24 hours, another interference pattern was taken as shown in Fig. 23(c). In Fig. 23(b) the angle α between the surface tilt of the twin and the basal plane was calculated from the fringe pattern and found to range from 3°45′ to 3°50′ along the twin (Appendix B). These values are within the experimental error of the theoretical value of 3°58′. The angle α changed to approximately 3° after annealing as measured from the fringe pattern shown in Fig. 23(c).

The trace of the same twin on the $(10\bar{1}0)$ surface was also observed. Fig. 24(a) shows the twin before annealing. After annealing at 200°C for 24 hours, the twin disappeared completely. The specimen was then etched. A trace of dislocations was found to have been left behind by the twin, as shown in Fig. 24(b).

3.7 Annealing of small twins

Twins ranging from 1 to 5 micron in thickness were generated by scratching the (0001) surface of the specimen with a razor blade. Fig. 25(a) shows many of such freshly introduced small twins. Fig. 25(b) was taken without polishing the specimen after it was annealed at 200°C for 10 hours. It shows that one of the twins along with its surface tilt has disappeared completely. The thickness of this twin was approximately 1.4 micron.

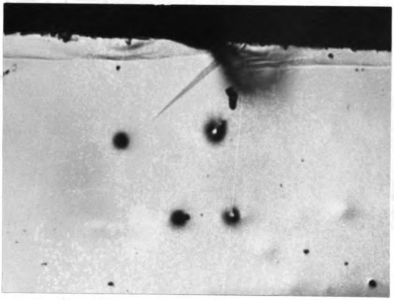

(a)

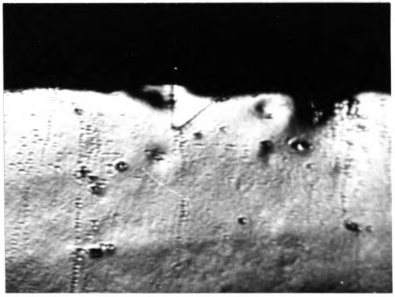

(b)

Fig. 24. Same twin as in Fig. 23, but viewed from the $(10\bar{1}0)$. 300X
(a) Fresh twin, corresponding to Fig. 23(a).
(b) After annealing, corresponding to Fig. 23(c), etched.

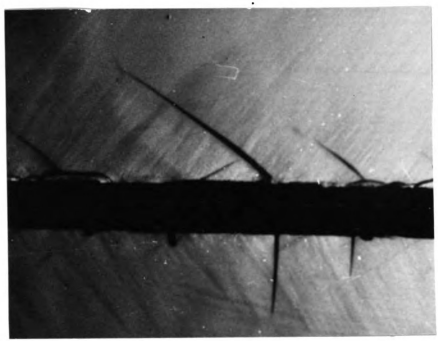

(a)

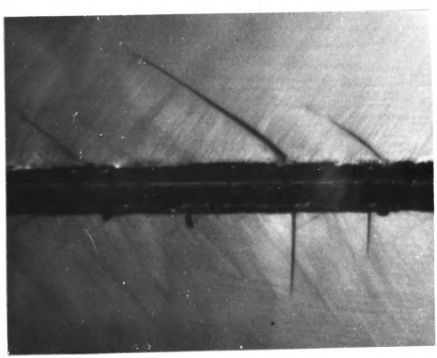

(b)

Fig. 25. Small twins on (0001) plane. 350X
(a) Before annealing.
(b) After annealing at 200°C for 10 hours.

IV. THEORY AND DISCUSSION

Deformation twin in zinc is a compound twin. In other words, the indices of K1 and K2 planes, and $\eta 1$ and $\eta 2$ directions are all rational[41]. In principle, a compound twin can be formed either by glide of dislocations on K1 with the rational direction $\eta 1$ parallel to the Burgers vector $\vec{b}_t$ of the twinning dislocation (type I), or by glide of dislocations on K2 with Burgers vector parallel to $\eta 2$ (type II). These two twinning modes are alternative ways of forming the same twin. Rais[42], Startsev et al[43] and Bengus[44] conducted a series of studies on the etch pit pattern of twinned calcite. They observed that there were pile-ups of dislocations at the twin interfaces and concluded that the twins were of type I, as introduced by Frank[45]. On the other hand, Bullogh[46] suggested that in substances with diamond cubic or hcp structures a twin interface is of the type II. Cahn[13] also pointed out another drawback of the type II twin model, in that it is inconsistent with the observation that in calcite the dislocation distribution along a twin interface changes as the interface migrates. The above objections raise some doubt in one's mind as to whether type II twins actually exist in crystals. Thus, in the following discussion of the twins in zinc, the type I model will be adopted.

4.1 The receding of the twin tip and the twin boundary energy

Deformation twins in zinc are observed to shrink, even at room temperature, and the rate of receding of the twin tip increases with increasing temperature. It is further observed that the twins in zinc recede lengthwise from the tip rather than transversely, as shown in Fig. 6. Figs. 7 and 8 show the sequence of the receding process. It can be seen clearly that, as the twin recedes, the tip becomes blunt at first. The receding rate of the tip will then decrease with the increase in height of the tip, and eventually become zero. The shape of the twin tip will become parallel-sided after it stops receding.

The receding of the twin tip during annealing can be described as a thermally activated polygonization process assisted by the twin interface energy. It appears that the energy of the coherent twin interface is the most important factor with regard to either the nucleation of the deformation twins[43] or the receding of the twin tips in zinc crystals. Yoo and Wei[36] estimated that the coherent twin boundary energy of the $(10\bar{1}2)$ $[10\bar{1}\bar{1}]$ type twins in zinc is of the order of 1.4 ± 0.4 ergs/cm^2, based on an idealized model of the twin with pointed tip. Using such a low value, the ease of the nucleation of deformation twins in zinc crystals was partially explained. An attempt is made here to give a more rigorous treatment of the twin interface energy, and to explain the thermodynamic instability of the deformation twins in zinc crystals.

4.1.1 A simplified two-dislocation model

Much of the behavior of the tip of a twin can be understood with a drastically simplified two-dislocation model. As shown in Fig. 26, let

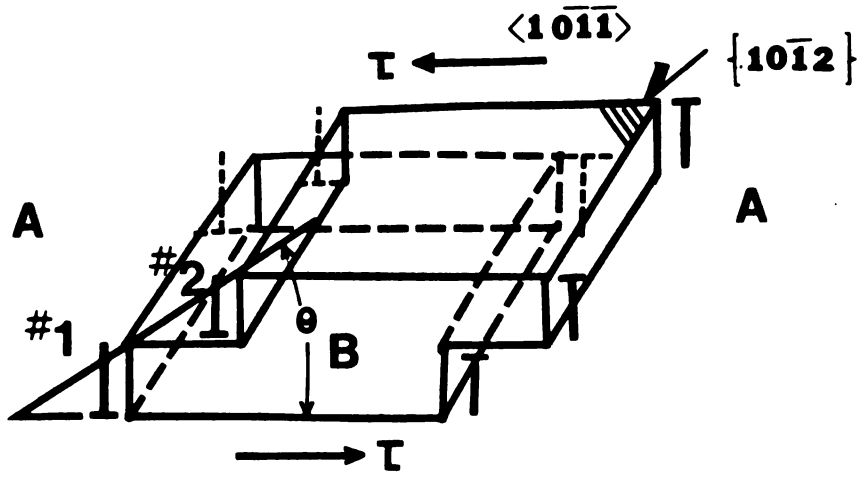

Fig. 26. Dislocation model of a two-layer twin.

A represent a hypothetical crystal lattice in which a two-layer twin B is being formed by the successive production of two pairs of twinning dislocations in the edge orientation lying in two neighboring $\{10\bar{1}2\}$ atomic planes. When a shear stress τ is applied, the dislocations of the opposite sign will move in opposite directions resulting in the expansion of the twinned region B.

When there is no obstacle in front of dislocation #1, its forward movement is hindered mainly by the tension of the two interfaces dragging behind it. Dislocation #2 is not under such restrictive forces, therefore it will soon catch up with dislocation #1. A dynamic equilibrium is then attained, and the two dislocations will move as a group in the direction dictated by the applied shear stress.

Considering a case in which the moving dislocation #1 is halted by an obstacle, let $\vec{b}_t$ be the Burgers vector of the twinning dislocation. The forces acting on dislocation #1 per unit length are:

$$pb_t + 2\gamma_t = \tau b_t + F_{2,1} \tag{1}$$

where pb_t is the Peierls-Nabarro force resisting the motion of the dislocation in terms of an equivalent stress p; γ_t is the coherent twin interface energy per unit area and is assumed to be independent of the twin thickness or the temperature; and $F_{2,1}$ is the component of the force per unit length acting on dislocation #1 by dislocation #2 in the twinning direction. It is further assumed that the velocity of the dislocation is low, so the energy dissipated by the moving dislocation can be neglected, and the stress field of the moving dislocation and its elastic strain energy remain the same as that of the dislocation at

rest. The forces acting on dislocation #2 are:

$$pb_t + \gamma_t + F_{1,2} = \tau b_t + \gamma_t \tag{2}$$

where $F_{1,2} = F_{2,1}$ is the component of the force acting on #2 by #1. The sum of (1) and (2)

$$2\gamma_t = 2b_t(\tau - p) \tag{3}$$

gives the external forces acting on the two dislocations. The difference of (1) and (2) gives

$$\gamma_t = F_{2,1} \tag{4}$$

provided that the maximum repulsive force $(F_{2,1})_{max.}$ between the two dislocations is numerically greater than γ_t. If, however, $(F_{2,1})_{max.}$ is smaller than γ_t, the two dislocations will travel in a configuration of minimal interaction energy, with dislocation #2 atop of dislocation #1.

Let a set of perpendicular axes be chosen so that the X-axis is in the $[\bar{1}011]$ direction, and Y-axis is perpendicular to the $(10\bar{1}2)$ glide plane. Let the position of dislocation #1 be at the origin, and dislocation #2 be at (x,d), where d is the distance between neighboring $\{10\bar{1}2\}$ atomic planes and is equal to 1.687 Å in zinc. Let $x_{2,1}$ be the distance between dislocation #1 and dislocation #2 along the X-axis.

The X-component of the interaction force is:

$$F_x = \frac{G b_t^2}{2\pi(1-\nu)} \frac{x_{2,1}(x_{2,1}^2 - y^2)}{(x_{2,1}^2 + y^2)^2} \tag{5}$$

Substituting $X = x_{2,1}/d$ and $y = d$ into (5), one obtains

$$F_x = \frac{G\, b_t^2}{2\pi d(1-\nu)} \frac{X(X^2 - 1)}{(X^2 + 1)^2} \tag{5a}$$

in which $G = 3.72 \times 10^{11}$ dyne/cm is the shear modulus of zinc. The maximum repulsive force per unit length between dislocation #1 and dislocation #2 is reached when $x_{2,1}/d = 2.41$ and is equal to:

$$(F_{2,1})_{max.} = 0.250 \frac{G\, b_t^2}{2\pi d(1-\nu)} \quad . \tag{5b}$$

Fig. 27 is a plot of $F_{2,1}$ as a function of X when $\gamma_t < (F_{2,1})_{max.}$ The angle θ of the tip of the twin is then a measure of γ_t. Such a configuration may or may not be thermodynamically stable, depending on how γ_t is compared with $F_{2,1}$. For instance, if the shaded area C in Fig. 2 is greater than the area D, the configuration of these two dislocations is then metastable. Enough thermal activation may cause dislocation #2 to overcome the maximum repulsive force between them and ride above dislocation #1. The energy of the system is then reduced by (C-D). This reduction in the interaction energy of the two dislocations is the "driving force" needed for such a process, essentially a polygonization process, to happen. The twin will then no longer have a pointed tip, but a blunt one. On the other hand, if C<D, there will be no driving force to push the two dislocations together, and hence they will be kept apart by the repulsion between them. The twin will have a pointed tip with an apex angle of $\theta = \cot^{-1} x_{2,1}/d$.

The interaction energy between the two dislocations as a function of X can be calculated by integrating eq. (5a),

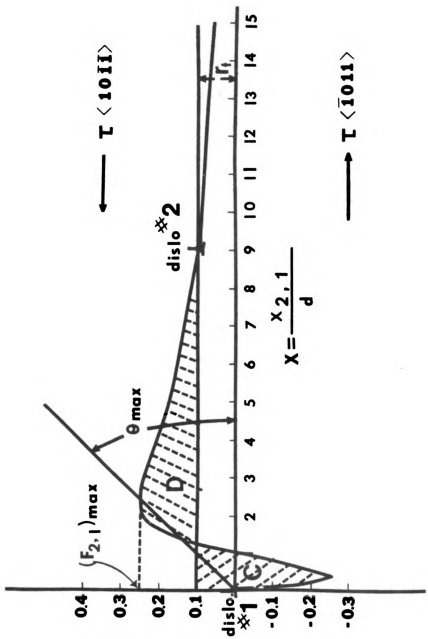

Fig. 27. Interaction force between two parallel dislocations in the edge orientation. X-component.

$$E_{2,1} = -\int_{o}^{X} F_{2,1}\, d\left(\frac{x_{2,1}}{d}\right) \tag{5c}$$

and is shown in Fig. 28, curve A.

The polygonization process can be helped by pinning down dislocation #2 and removing the applied shear stress. In such a case, dislocation #1 will be pulled back toward dislocation #2 by a force per unit length numerically equal to $2\gamma_t$ instead of γ_t. The interaction energy between the two dislocations is then represented by curve B in Fig. 28. The angle between such a pair of parallel-edge dislocations has to be smaller than $\cot^{-1} X_1$ for polygonization to take place. This initial condition for polygonization is achieved either by an applied stress, or by the presence of other dislocations, or both.

In Fig. 28, X_1 is approximately equal to 3.2, corresponding to $\theta \cong \cot^{-1} 3.2 = 17^{o}$. In other words, for a two-layer twin with a pointed tip, the apex angle of the tip must be smaller than 17^{o}. Otherwise, the tip will become blunt when there is enough thermal activation.

When the applied shear stress τ is gradually reduced, both dislocations will gradually slow down, stop, and eventually move backward. Let τ_1 be the applied stress at which the dislocations start to move backward. One may analyze the situation as before, and obtain

$$\gamma_t = F_{2,1} = (\tau_1 + p)\, b_t \tag{5d}$$

This means that unless these two dislocations polygonize, they will remain at the same configuration regardless of whether they are moving forward, or backward, or standing still, held by a stress $\tau_2 = \gamma_t / b_t$ in an otherwise perfect crystal lattice.

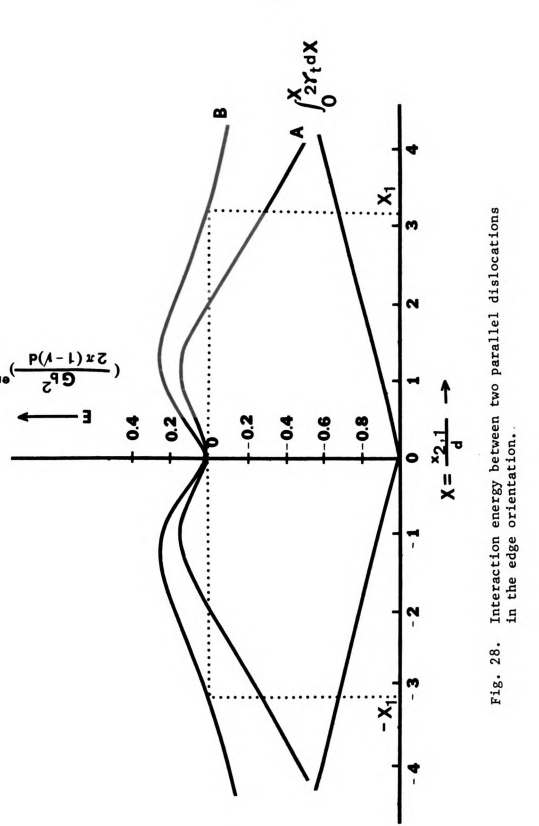

Fig. 28. Interaction energy between two parallel dislocations in the edge orientation.

The Peierls stress p is of the order of 10^{-4} to 10^{-2} G; the higher value is associated with covalent crystals, and the lower value, close-packed metals[48]. The Peierls force for the twinning dislocations in zinc is therefore on the low side. If we take $p \cong 10^{-4}$ G, then

$$pb_t = 3.72 \times 10^{11} \times 10^{-4} \times 0.235 \times 10^{-8} \text{ erg/cm}^2$$

$$= 0.087 \text{ dyne/cm} .$$

In the presence of enough thermal activation, the polygonization process probably will start by forming a pair of kinks along the dislocation line #1, as shown in Fig. 29. This pair of kinks will move apart over the entire length of dislocation #1 and cause it to move toward dislocation #2. The process will continue until these two dislocations reach their equilibrium position, with one riding on top of the other. By so doing, the twin recedes, with a decrease in the interaction energy of the two dislocations. The shape of the twin tip will change from pointed to blunt. The process described above is essentially a polygonization process assisted by the tension of the twin interfaces. It will happen only when the twinning dislocations are purely or mainly of an edge character. Higher temperature reduces the Peierls potential by blurring the lattice periodicity, increases the amplitude of the vibrating dislocation line, increases the probability of forming the kinks, and hence increases the pologonization rate.

4.1.2 Dislocation model of a many-layer twin

Since an observable twin must have many layers, a more general model is needed. A dislocation model representing the tip of a receded many-layer twin is shown in Fig. 30. Assuming that there are m twinning

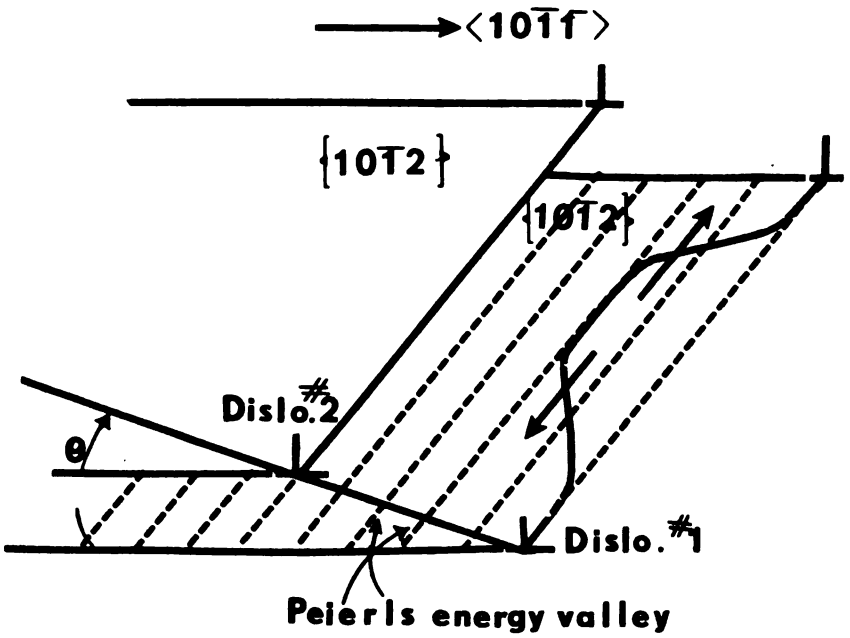

Fig. 29. The polygonization process of a two-layer twin.

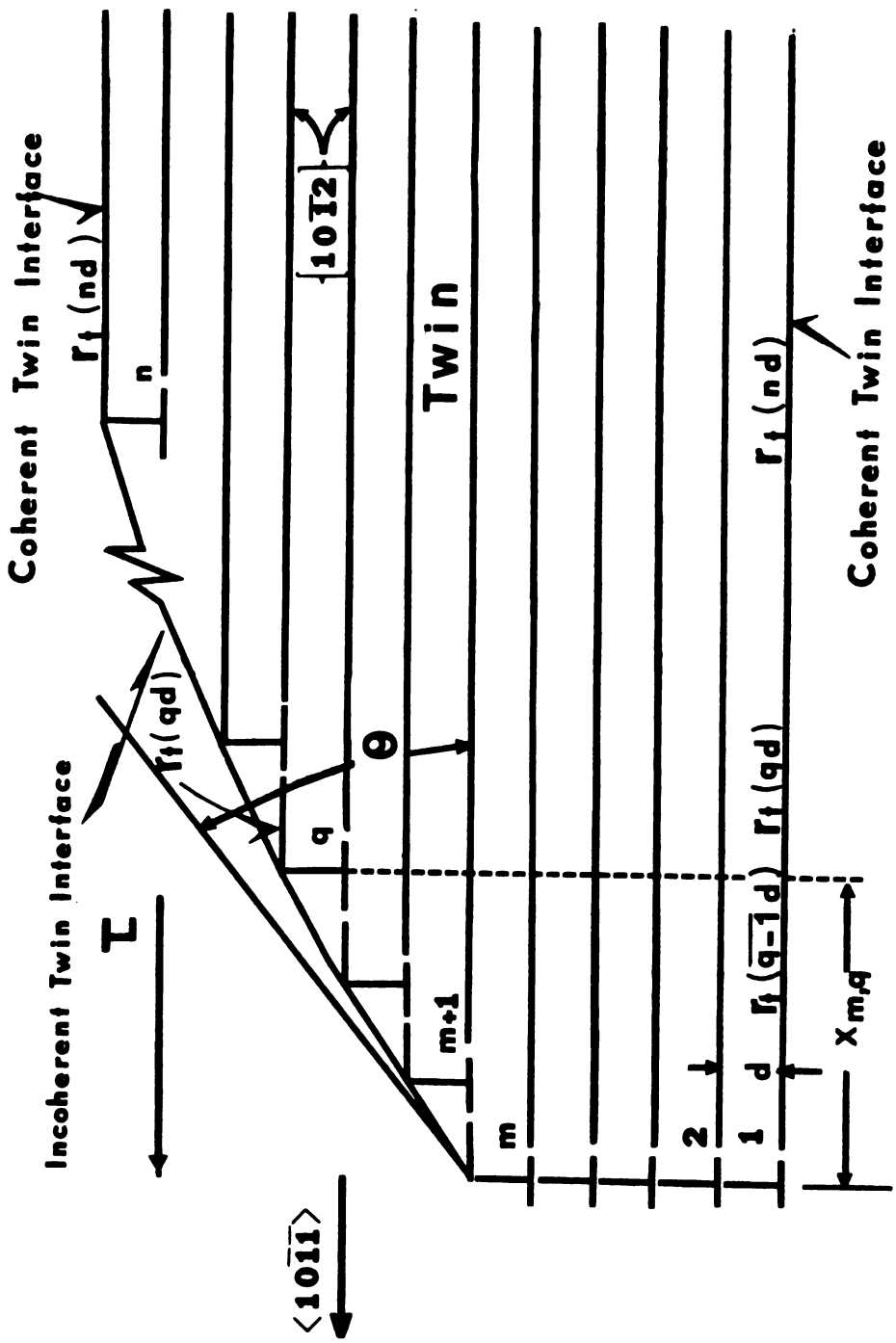

Fig. 30. Dislocation model of a many-layer twin.

dislocations arranged in a vertical wall followed by (n - m) dislocations forming a sort of "pile-up" on successive atomic planes, let a set of rectangular Cartesian axes be chosen so that the X-axis is parallel to the $[10\bar{1}\bar{1}]$ direction, and Y-axis is perpendicular to the twinning plane. Let d be the spacing of the $(10\bar{1}2)$ plane and $x_{i,j}$ be the distance between the ith and jth dislocations measured along the X-axis. Let $F_{i,j}$ be the X-component of the interaction force experienced by the jth dislocation in the stress field of the ith dislocation, and θ be the angle between the tangent of the incoherent twin interface at the tip and the coherent twin interface. Furthermore, the twin is assumed to be of unit thickness measured normally to the plane of the drawing, and the crystal is perfect except for the presence of the twin. It is also assumed that the linear, isotropic, elasticity theory is valid.

Because the angle of the twin tip is small and the spacing of the glide plane is also small, the distance between the twinning dislocations in the incoherent boundary measured along the X-axis can be considered as being equal to the corresponding distance in a linear dislocation pile-up as a first approximation. Since the distance between neighboring dislocations in such a pile-up increases as the dislocations are further and further away from the leading dislocation, the incoherent interface at the tip will be curved as shown in Fig. 30. In order to examine the interaction forces between the (m+1) th dislocation and the [n - (m+1)] dislocations following it, certain assumptions will have to be made.

Eshelby, Frank and Nabarro[49] investigated the equilibrium position of n dislocations in a piled-up group under a constant applied stress.

Mitchell, Hecker and Smialek[50] calculated the equilibrium position for n = 1 to 99 by equating the first derivatives of the nth Laguerre polynomial to zero. The values of the equilibrium positions of the dislocations in such a pile-up are listed in Appendix C.

The resolved shear stress acting on the twin plane in the twinning direction when the twin grows was measured by Chyung and Wei[47] to be 130 ± 50 g/mm^2. The low value of 80 g/mm^2 is used for calculating the equilibrium position of the dislocations in a linear pile-up. As defined earlier, the position of dislocation #1 is at the origin of the rectangular Cartesian coordinate, dislocation #2 is at $(x_{2,1}, d)$, the qth dislocation is then at $[x_{q,1}, (q-1)d]$, etc. Thus the distance between the qth and the (q+1) th dislocation along the X-axis will be $(x_{q+1} - x_{q,1})$, and the distance along the Y-axis will be d.

Fig. 31 shows the total force exerted by the dislocations in the pile-up on the (m+1) th dislocation as a function of m. It shows that $\sum_{j=m+2}^{99} F_{j,m\pm1}$ drops 86% when m increases from 1 to 10.

It is assumed that the system in Fig. 30 is on the verge of moving forward under an applied shear stress τ acting on the $\{10\bar{1}2\}$ twinning plane in the $\langle 10\bar{1}\bar{1}\rangle$ direction. Let all the dislocations be straight, parallel to each other, extend over the entire thickness of the crystals, and be in the edge orientation. It is also assumed that the energy of the twin interface is, in general, a function of the local height of the twin, qd, or $\gamma_t = \gamma_t(qd)$. The X-components of the forces acting on the qth dislocations are:

Fig. 31. Interaction forces between the (m+1) th dislocation and the [99-(m+1)] dislocations in the boundary. X-component.

$$\sum_{j=1}^{q-1} F_{j,q} + 2\gamma_t(qd) + pb_t = \tau b_t + 2\gamma_t(\overline{q-1}d) + \sum_{j=q+1}^{n} F_{j,q}$$

or

$$2\gamma_t(qd) - 2\gamma_t(\overline{q-1}d) = (\tau - p)b_t - \sum_{j=1}^{q-1} F_{j,q} + \sum_{j=q+1}^{n} F_{j,q} \qquad (6)$$

The sum of the X-components of the forces acting on the leading group of m dislocations gives:

$$2\gamma_t(md) = m(\tau - p)b_t + \sum_{j=m+1}^{n} \sum_{k=1}^{m} F_{j,k} \quad . \qquad (7)$$

For the (m+1) th dislocation, one obtains:

$$2\gamma_t(\overline{m+1}d) - 2\gamma_t(md) = (\tau - p)b_t - \sum_{j=1}^{m} F_{j,m+1} + \sum_{j=m+2}^{n} F_{j,m+1} \qquad (8)$$

For the last dislocation in the system, the nth, the sum of the forces gives:

$$2\gamma_t(nd) - 2\gamma_t(\overline{n-1}d) = (\tau - p)b_t - \sum_{j=1}^{n-1} F_{j,n} \quad . \qquad (9)$$

There are altogether (n-m+1) such equations. The sum of all the (n-m+1) equations gives again the total external forces acting on the system:

$$2\gamma_t(nd) = n(\tau - p)b_t \quad . \qquad (10)$$

If n is sufficiently large so that $\gamma_t(nd) \cong \gamma_t(\infty)$, the true coherent twin interface energy, one obtains:

$$\gamma_t(\infty) \cong \frac{n}{2}(\tau - p)b_t \quad , \qquad (11)$$

and

$$\tau - p \approx \frac{2\gamma_t(\infty)}{nb_t} \tag{12}$$

becomes very small.

When τ is gradually reduced to τ_1 at which point the twin starts to shrink due to the tension of the twin interfaces, one obtains:

$$2\gamma_t(nd) = n(\tau_1 + p)b_t \ , \tag{13}$$

Solve for $\gamma_t(nd)$ from eq. (10) and (13) assuming n is large:

$$\gamma_t(\infty) \cong \frac{n}{4}(\tau + \tau_1)b_t \ . \tag{14}$$

It may appear that $\gamma_t(\infty)$ can be evaluated from this equation by applying stresses τ and τ_1 and observing the movement of the twin interface. However, one may expect unsurmountable difficulties in such an experiment. One may try to obtain some limiting values of γ_t based on the following analysis. The difference of eq. (7) and (8) gives:

$$\begin{aligned} & 2\gamma_t(md) - 2[\gamma_t(\overline{m+1}d) - \gamma_t(md)] \\ = \ & (m-1)(\tau-p)b_t + \sum_{j=m+1}^{n}\sum_{k=1}^{m} F_{j,k} + \sum_{j=1}^{m} F_{j,m+1} - \sum_{j=m+2}^{n} F_{j,m+1} \end{aligned} \tag{15}$$

Since

$$F_{j,m+1} = \frac{Gb_t^2}{2\pi(1-\nu)} \frac{x_{j,m+1}\,(x_{j,m+1}^2 - \overline{m+1-j}^2 d^2)}{(x_{j,m+1}^2 + \overline{m+1-j}^2 d^2)^2} \ , \tag{16}$$

Let

$$D = \frac{Gb_t}{2\pi(1-\nu)} \ , \tag{17}$$

$$X_{i,j} = \frac{x_{i,j}}{d} \tag{18}$$

and substituting into eq. (16) one obtains

$$\sum_{j=1}^{m} F_{j,m+1} = \frac{Db_t}{d}\left[\sum_{j=1}^{m} \frac{X_{m,m+1}(X_{m,m+1}^2 - \overline{m+1-j}^2)}{(X_{m,m+1}^2 + \overline{m+1-j}^2)^2}\right] . \tag{19}$$

According to Nabarro[51], the force between a dislocation and an infinite wall when the dislocation glides out of the wall is:

$$F_x = -\frac{Db_t}{x}\left(1 - \frac{\pi^2 x^2}{d^2} / \sinh^2 \frac{\pi x}{d}\right) .$$

In the present case, when $m \to \infty$, the force between this wall and the (m+1) th dislocation can be written as:

$$\sum_{j=1}^{m\to\infty} F_{j,m+1} = \frac{1}{2} F_x = -\frac{Db_t}{2dX}(1 - \pi^2 X^2 / \sinh^2 \pi X) . \tag{19a}$$

Fig. 32 shows $F_{m+1,j}$ as a function of $X_{m+1,j}$ for $j = m, m-1, m-2, m-3$ and m-4 respectively. Fig. 33 shows $\sum_{j=1}^{m} F_{m+1,j}$ as a function of $X_{m+1,j}$, for $m = 1,2,3,10,50,500,1000$ and as $m \to \infty$.

When m is much smaller than n, one can neglect $(m-1)(\tau-p)b_t$ in eq. (15) and write:

$$S_m = \frac{1}{2}\sum_{j=1}^{m} F_{j,m+1} + \delta \tag{20}$$

where

$$S_m = \gamma_t(md) + \eta \tag{21}$$

$$\eta = \gamma_t(md) - \gamma_t(\overline{m+1}d) \tag{22}$$

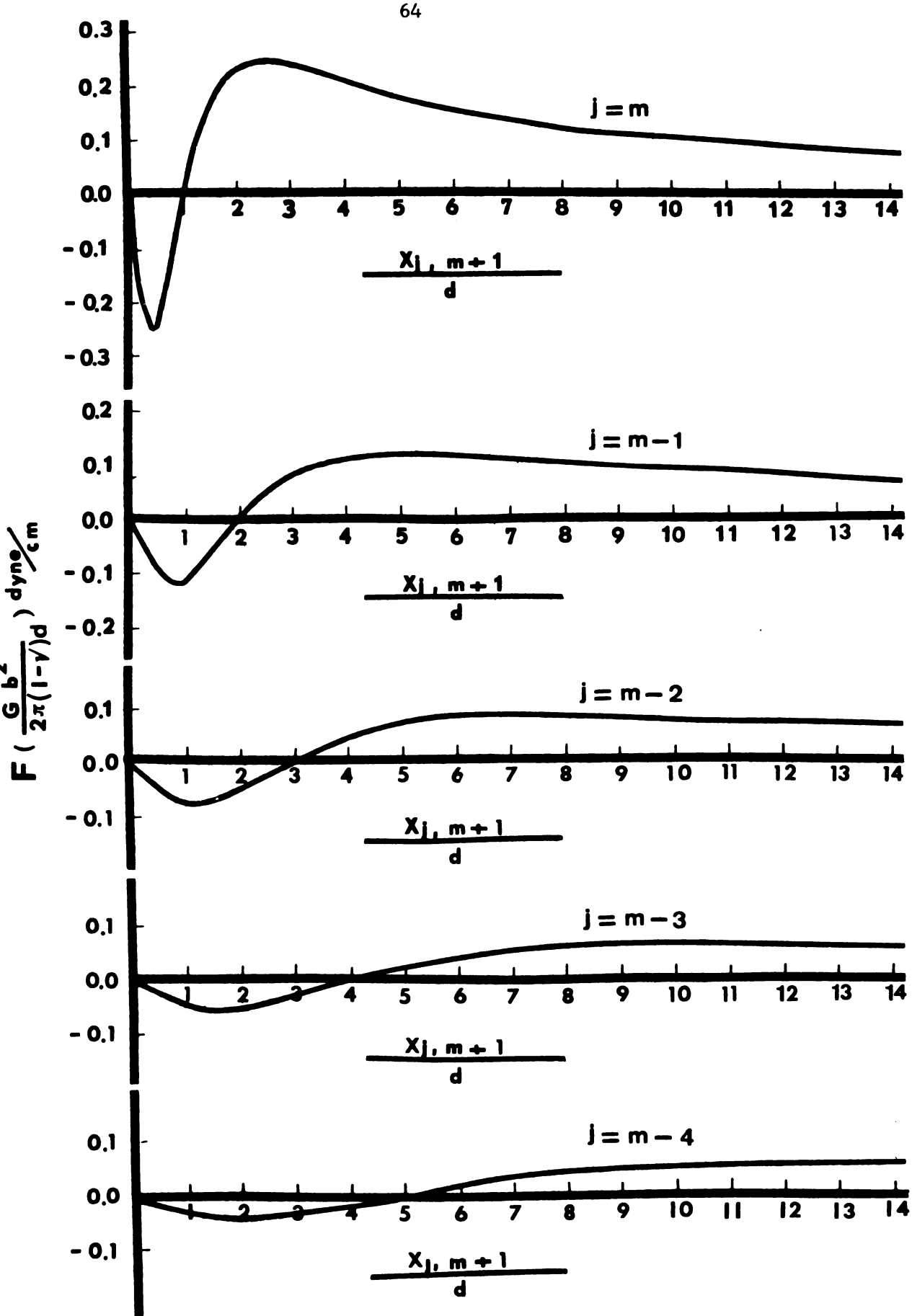

Fig. 32. Interaction forces between the (m+1) th dislocation and the j th dislocation. X-component.

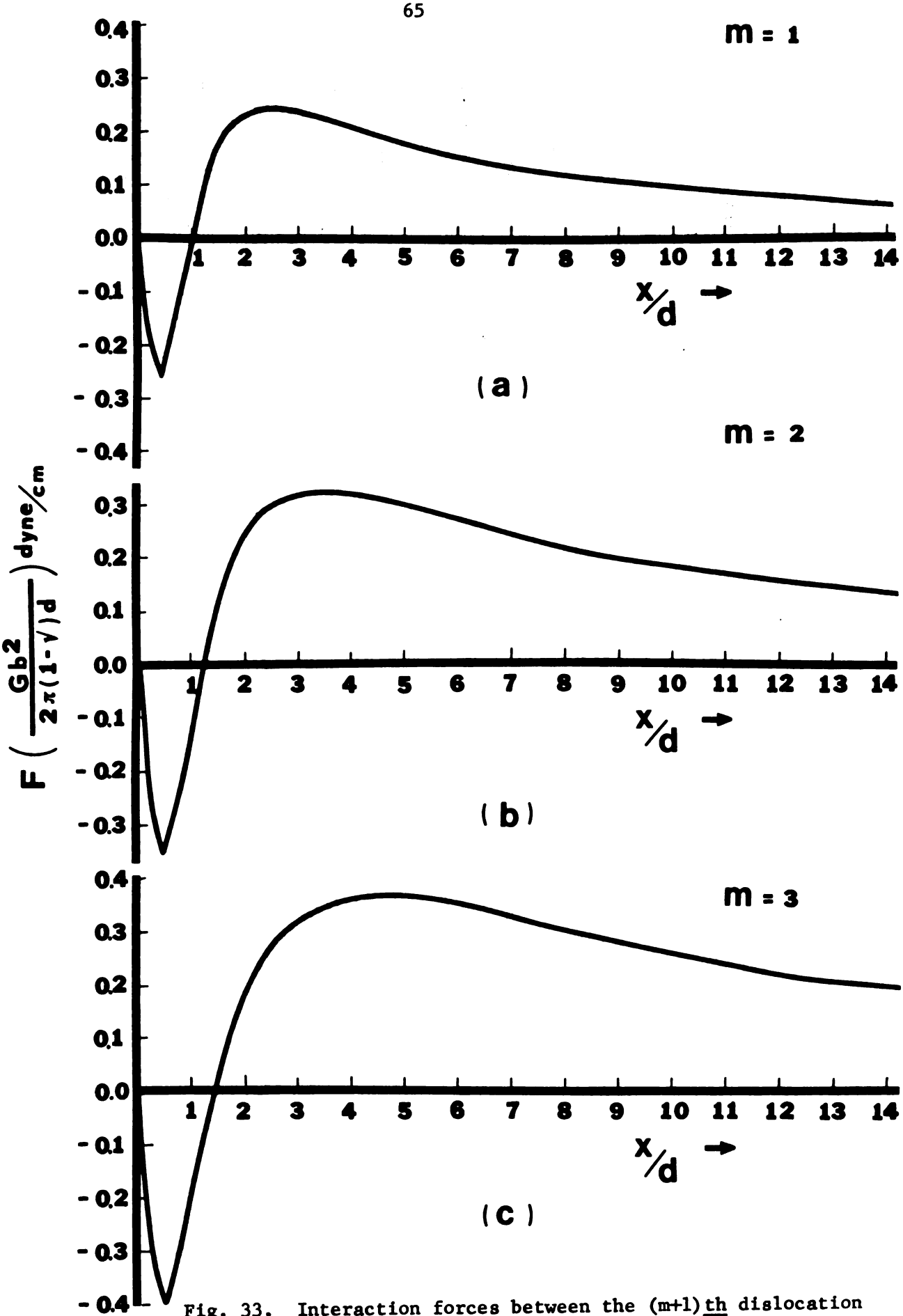

Fig. 33. Interaction forces between the (m+1)th dislocation and the m -dislocation wall. X-component.

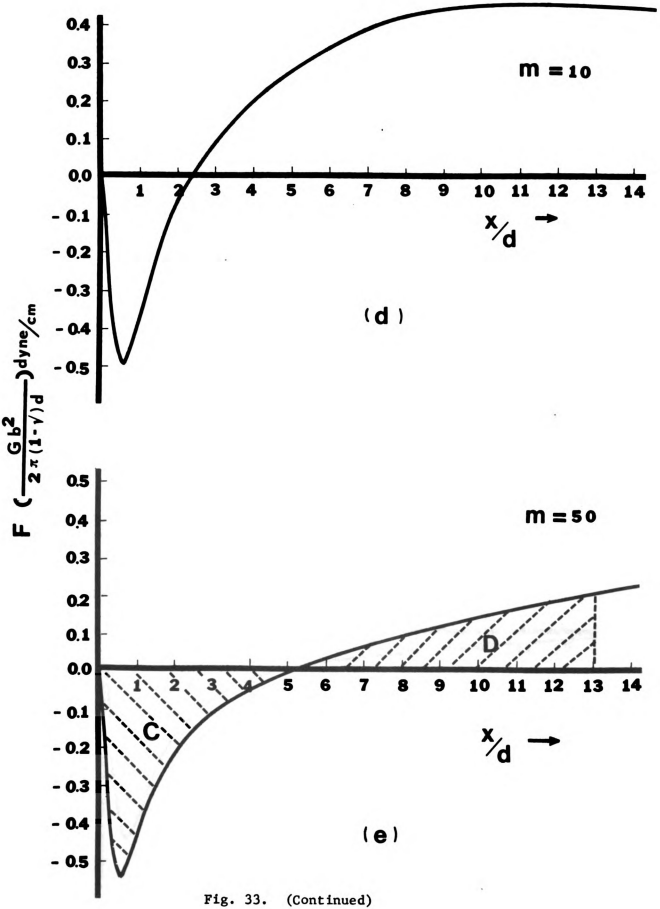

Fig. 33. (Continued)

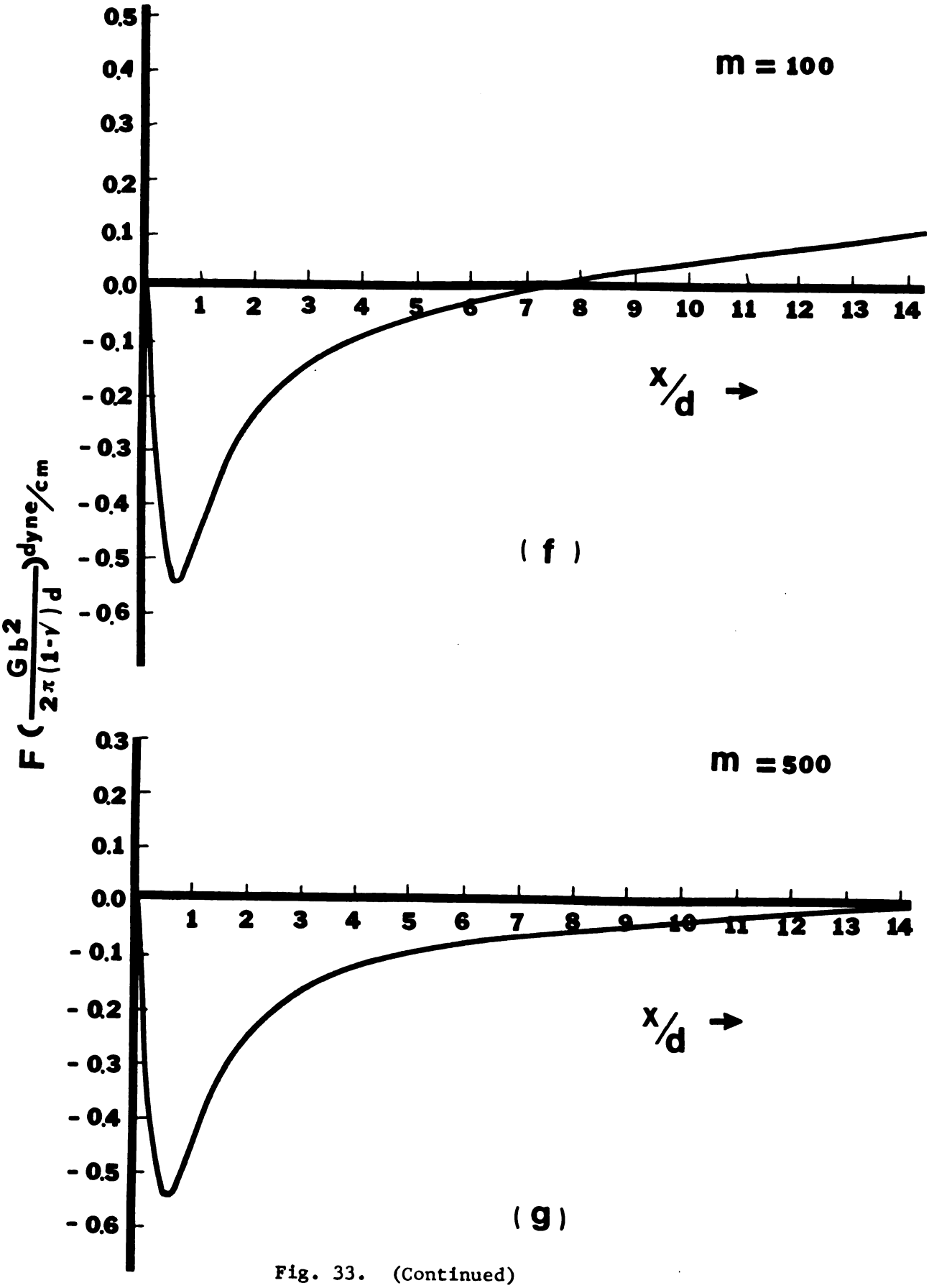

Fig. 33. (Continued)

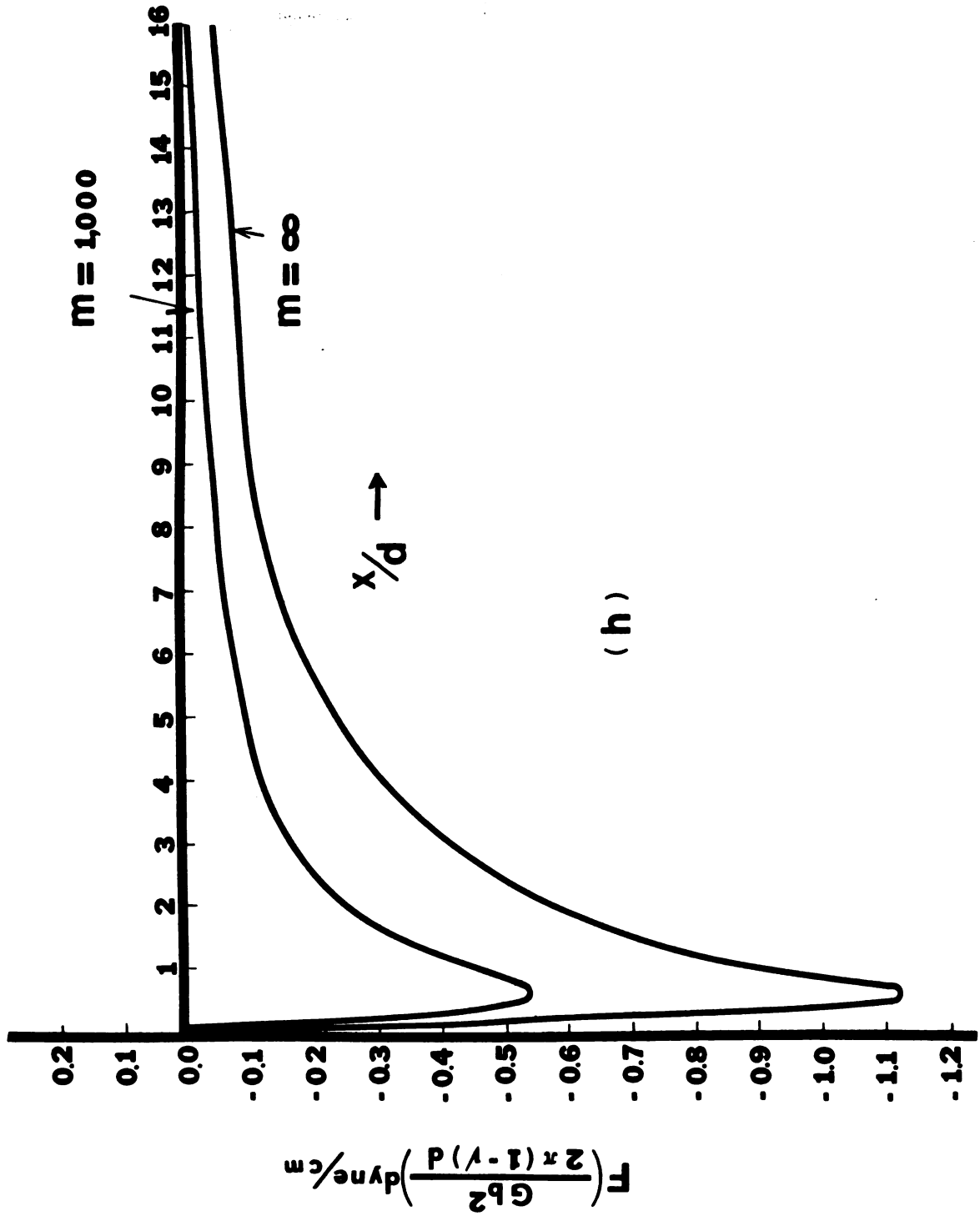

Fig. 33. (Continued)

$$\delta = \frac{1}{2}\left[\sum_{j=m+1}^{n}\sum_{k=1}^{m} F_{j,k} - \sum_{j=m+2}^{n} F_{j,m+1}\right] . \tag{23}$$

One may also obtain from eqs. (15), (21), (22):

$$S_m = \sum_{j=1}^{m} F_{j,m+1} - \epsilon \tag{24}$$

where

$$\epsilon = \frac{1}{2}\sum_{j=m+2}^{n}\left[F_{j,m+1} - \sum_{k=1}^{m} F_{j,k}\right] \tag{25}$$

and

$$F_{i,j} = F_{j,i} .$$

Also, eqs. (20) through (24) give

$$\delta + \epsilon = \frac{1}{2}\sum_{j=1}^{m} F_{j,m+1} . \tag{26}$$

When a growing twin has a pointed tip or m=1, equations (20) through (26) then become:

$$S_1 = \frac{1}{2} F_{1,2} + \delta \tag{20a}$$

$$S_1 = \gamma_t(d) + \eta \tag{21a}$$

$$\eta = \gamma_t(d) - \gamma_t(2d) \tag{22a}$$

$$\delta = \frac{1}{2}\left[\sum_{j=2}^{n} F_{j,1} - \sum_{j=3}^{n} F_{j,2}\right] \tag{23a}$$

$$S_1 = F_{1,2} - \epsilon \tag{24a}$$

$$\epsilon = \frac{1}{2} \sum_{j=3}^{n} [F_{j,2} - F_{j,1}] \tag{25a}$$

$$\delta + \epsilon = \frac{1}{2} F_{1,2} \quad . \tag{26a}$$

Since $\sum_{j=2}^{n} F_{j,1} \geq \sum_{j=3}^{n} F_{j,2}$ and $\epsilon > 0$, one obtains

$$0 \leq \delta < \frac{1}{2} F_{1,2} \tag{27}$$

$$0 < \epsilon < \frac{1}{2} F_{1,2} \quad . \tag{28}$$

From eqs. (24a) and (21a) one obtains

$$\frac{1}{2} F_{1,2} + \delta = S_1 = F_{1,2} - \epsilon \quad ,$$

which leads to

$$\frac{1}{2} F_{1,2} < \frac{1}{2} F_{1,2} + \delta = 2\gamma_t(d) - \gamma_t(2d) = F_{1,2} - \epsilon < F_{1,2} \quad . \tag{29}$$

If the angle θ at the twin tip can be measured experimentally, $F_{1,2}$ can then be read out from Fig. 27. $S_1 = 2\gamma_t(d) - \gamma_t(2d)$ is definitive within a factor of two.

It may be assumed that $\gamma_t(\infty) < \gamma_t(2d) < \gamma_t(d)$, meaning that the coherent twin interface becomes more and more stable as the number of layers in the twin increases. It follows that

$$\eta = \gamma_t(d) - \gamma_t(2d) > 0$$

and

$$\gamma_t(\infty) < \gamma_t(d) = S_1 - \eta = F_{1,2} - \epsilon - \eta$$

or

$$\gamma_t(\infty) < F_{1,2} - \epsilon - \eta \quad .$$

From eq. (29)

$$S_1 = 2\gamma_t(d) - \gamma_t(2d) = \gamma_t(d) + \eta$$

$$\frac{1}{2} F_{1,2} + \delta - \eta = \gamma_t(d) = F_{1,2} - \epsilon - \eta \quad ,$$

so that

$$\gamma_t(\infty) < \gamma_t(d) < F_{1,2} - \epsilon - \eta \tag{30}$$

and

$$\gamma_t(\infty) < \gamma_t(d) > \frac{1}{2} F_{1,2} + \delta - \eta \quad . \tag{31}$$

Neglecting $(\tau - p)b_t$, equation (8) becomes

$$\gamma_t(d) - \gamma_t(2d) = \eta = \frac{1}{2} (F_{1,2} - \sum_{j=3}^{n} F_{j,2}) \tag{32}$$

and therefore η must be smaller than $1/2\ [(F_{1,2})_{max} - \sum_{j=3}^{n} F_{j,2}]$.

If η is greater than $1/2\ [(F_{1,2})_{max} - \sum_{j=3}^{n} F_{j,2}]$, equilibrium cannot be established for $m = 1$. The interface at the tip of the twin will pull the second dislocation forward until it rides above the leading dislocation. The case becomes one of $m = 2$. Since most of the deformation twins in zinc crystals are observed to have pointed tips, one can then set a limit of the values of the coherent twin boundary energy to lie between $1/2\ F_{1,2}$ and $F_{1,2}$ based on equations (30) and (31), i.e.,

$$1.4 \pm 0.4 \text{ ergs/cm}^2 \leq \gamma_t \leq 2.8 \pm 0.8 \text{ ergs/cm}^2$$

for the $(1\bar{1}02)\ \langle 1\bar{1}0\bar{1}\rangle$ twin system in zinc crystals.

4.1.3 Change in shape of the twin during annealing

When the twin begins to recede during annealing, the twin interface energy is the main driving force. The dislocation at the tip of the twin is pulled backward by the two interfaces with a force numerically equal to $2\gamma_t$. It is a polygonization process assisted by the twin interfaces, in addition to the interaction of the twinning dislocation at the tip, and, as a result, there is a net decrease in the energy of the system. The backward pull of $2\gamma_t$ is essentially constant, but the resistance of the lattice to the backward movement of the polygonized wall is proportional to m. It will stop when $2\gamma_t \cong mpb_t$. Using $\gamma_t = 1.4 \sim 2.8$ ergs/cm^2, one obtains $m = 30 \sim 60$.

When m increases, the interaction between the $(m+1)$ th and the group of m dislocations in the wall becomes important. As shown in Figs. 32 and 33, the interaction is a short range attraction and a long range repulsion when m is small. When m increases, the repulsion between the $(m+1)$ th dislocation and the dislocation wall will gradually decrease and finally change into an attractive force. In the meantime, the range of the attractive interaction and the magnitude of the attractive force will both increase.

When the angle of the twin tip lies between 4^o and 13^o, as normally observed in zinc crystals, Fig. 33 indicates that, as the number of dislocations in the wall reaches 500 or more, the $(m+1)$ th dislocation will experience an attractive force due to the stress field of the dislocation wall at the tip. It will move forward and polygonize if this attractive force is larger than the lattice resistance. Between $m = 30 \sim 60$ and $m = 500$, even though the interaction between the m dislocations in the polygonized wall and the $(m+1)$ th dislocation is

repulsive at x/d = 13, polygonization can still proceed by thermal activation if there is a net decrease in the total energy of the system. As shown in Fig. 33(e), the shaded areas C and D are approximately equal. Polygonization is possible if the position of the (m+1) th dislocation $x/d \leq 13$. In reality, the forward repulsion acted on the (m+1) th dislocation by the subsequent dislocations in the pile-up as shown in Fig. 31 will facilitate the polygonization process. This process will continue and eventually the neighboring region of the wall will be depleted of the twinning dislocations. The process will stop when the distance between the mth and the (m+1) th dislocation becomes so large that the attractive force between them is insufficient to overcome the lattice friction to the motion of the (m+1) th dislocation. A metastable configuration is then reached, and the twin will have a blunt and parallel-sided tip as shown in Fig. 7.

4.2 Characteristics of dislocations left by the receded twin

As pointed out earlier in Chapter I, section 1.2, basal dislocations must have been formed in the accommodation zone with their negative parts being adjacent to the twin boundary during the twinning. In Fig. 11, a large number of polygonization walls consisting of basal dislocations can be observed. Fig. 22 shows a scanning electron micrograph of a freshly twinned crystal. Many dislocations can be seen near the tip region of the twin.

Fig. 14 shows the trace left by the receded twin on both the front and back surfaces of the specimen. The similarity of these two pictures indicates that the dislocations in the trace must extend over the entire thickness of the specimen and lie on a set of parallel planes.

The dislocations in the trace cannot be basal dislocations since they do not polygonize in the direction perpendicular to the basal plane. Fig. 15 shows that under the specific loading conditions described previously to produce a larger number of $(11\bar{2}2)$ $[20\bar{2}\bar{3}]$ second order pyramidal dislocations near the trace and the twin tip, the trace can still be seen as a distinctive line among the second order pyramidal dislocations, not moved by the applied stress. It is, therefore, unlikely that the dislocations in the trace are second order pyramidal dislocations.

The scanning electron micrographs shown in Figs. 16 through 19 indicate that the trace is really a continuation of dislocation in the neighborhood of the twin boundary.

Figs. 16 and 18 show that the density of the dislocations in the trace is different from that in the twin boundary. Since the shape of the etch pips is related to the character of the dislocations, the different types of etch pips existing in the twin boundary would indicate that there are more than one type of dislocations in the boundary. The dislocations left behind by the receded twin are of one particular type.

Dislocations can only polygonize into a wall perpendicular to the Burgers vector of the dislocations. Figs. 11 and 12 show that the tip of the trace has polygonized after prolonged annealing. The polygonized wall revealed by the etch pips on such a prism plane is in a direction parallel to the trace of the basal plane. The same phenomenon can also be seen in Figs. 12, 13 and 20. Fig. 13 also shows the sequence of the polygonization process.

The above observations point out the fact that the Burgers vector of the dislocations in the polygonized wall must be $\vec{c}$. These dislocations are neither basal nor second order pyramidal dislocations. Since the slip traces in the twin were observed to be parallel to the trace of the basal plane in the twin, one can assume that the most probable slip dislocations in the twin are basal dislocations. An $a/3[\bar{2}110]$ or $(-a_3)$ basal dislocation in a $(1\bar{1}02)[1\bar{1}0\bar{1}]$ twin can penetrate the twin boundary and be incorporated into the matrix to become a $a/3[\bar{1}\bar{1}23]$ or $(c + a_3)$ dislocation as described by Yoo and Wei[52]. Such a dislocation is constrained to move on the $(1\bar{1}00)$ plane in the matrix. It can not move far away from the twin boundary because $(1\bar{1}00)$ is not an active slip plane. Since there are many basal dislocations near the twin boundary, as described earlier, the annealing will assist the reaction between the basal dislocations and the prismatic dislocations near the twin boundary. Thus, the following reaction could have happened during the annealing:

$$(\vec{c} + \vec{a}_3) + (-\vec{a}_3) \longrightarrow \vec{c} \tag{37}$$

or

$$a/3[\bar{1}\bar{1}23] + a/3\ [11\bar{2}0] \longrightarrow a[0001]\ . \tag{38}$$

As pointed out by Yoo and Wei[52], the $a/3[\bar{1}\bar{1}23]$ dislocation would lower its energy if it dissociates into two partial dislocations. Thus, reaction (38) can be written as:

$$2 \times a/6[\bar{1}\bar{1}23] + a/3[11\bar{2}0] \longrightarrow a[0001]. \tag{39}$$

Furthermore, $a[\vec{c}]$ dislocation is also likely to dissociate into two partial dislocations:

$$a[0001] \longrightarrow a/2\ [0001] + a/2\ [0001]\ . \tag{40}$$

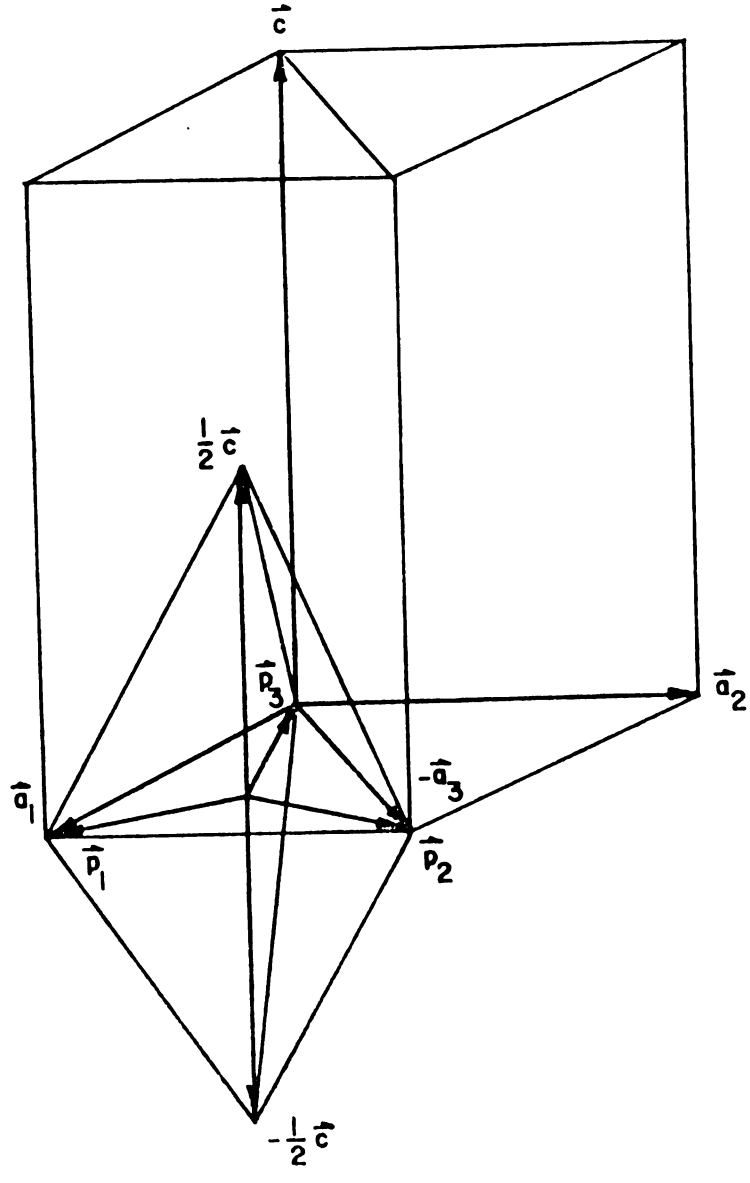

Fig. 34. Burgers vectors in hexagonal close-packed lattice.

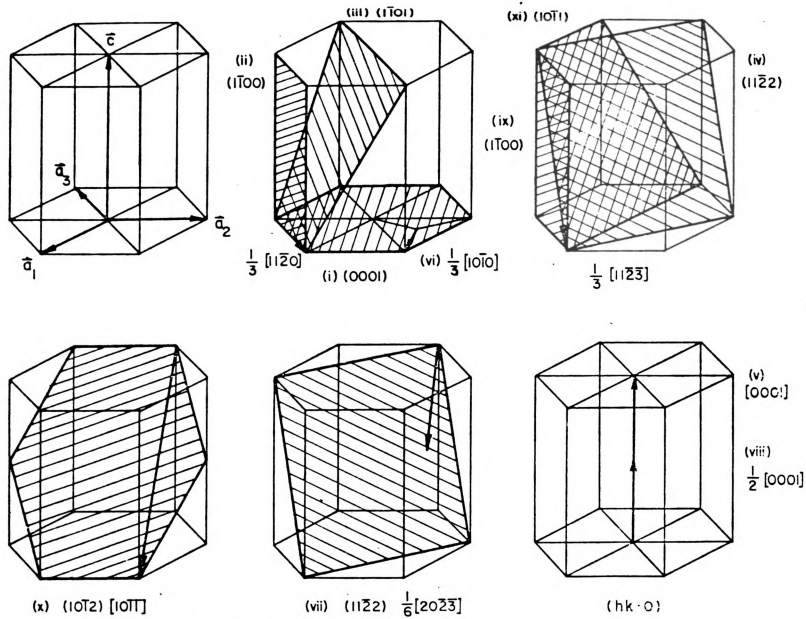

Fig. 35. Slip systems and twin system in zinc crystal.

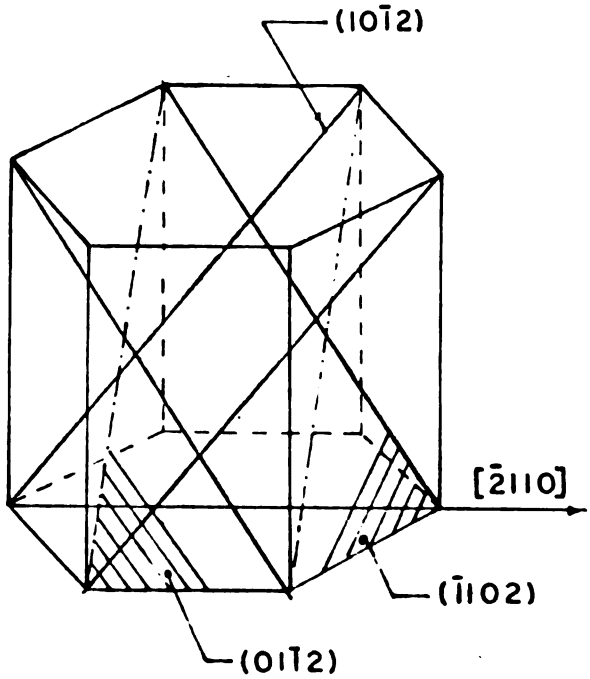

$$\begin{bmatrix}(T_1,t_1);\ (\bar{1}012)\ [\bar{1}01\bar{1}]\\ (T_4,t_4);\ (\bar{1}102)\ [\bar{1}10\bar{1}]\end{bmatrix}$$

$$\begin{bmatrix}(T_2,t_4);\ (01\bar{1}2)\ [01\bar{1}\bar{1}]\\ (T_5,t_5);\ (0\bar{1}12)\ [0\bar{1}1\bar{1}]\end{bmatrix}$$

$$\begin{bmatrix}(T_3,t_3);\ (1\bar{1}02)\ [1\bar{1}0\bar{1}]\\ (T_6,t_6);\ (10\bar{1}2)\ [10\bar{1}\bar{1}]\end{bmatrix}$$

Fig. 36. Reference twin systems.

The true representative reaction can be obtained by adding equations (39) and (40):

$$2 \times a/6[\bar{1}\bar{1}23] + a/3[11\bar{2}0] \longrightarrow a/2[0001] + a/2\ [0001] \qquad (41)$$

or

$$2 \times 1/2\ (\vec{c} + \vec{a}) + (-\vec{a}) \longrightarrow 2 \times (\vec{c}/2) \qquad (42)$$

The resulting dislocations would lie on the prism plane of the matrix and have Burgers vector $\vec{c}/2[0001]$. This incorporation process is shown in Fig. 38. Fig. 37 shows schematically the dislocations in the trace before and after polygonization. By using the criterion of the square of magnitude of the Burgers vector, there is a reduction in energy from

$$2 \times 1.054^2\ a^2 + a^2 \rightarrow 2 \times 0.928\ a^2$$

$$\Delta E = \frac{E_2 - E_1}{E_1} = \frac{1.72 - 3.22}{3.22} = -46.6\%$$

thus equation (41) is energetically favorable.

The dislocations lying in the prismatic plane with Burgers vector $1/2\ \vec{c}$ are known to be inactive in zinc crystals at room temperature. The present results substantiate such observations in the literature[53].

4.3 Surface tilt left by the receded twins

In principle, deformation twinning is crystallographically reversible. If no accompanying slip is involved, twinning itself will produce a surface tilt angle α of $3^{\circ}58'$ as it is fixed by the crystallography of zine. When the twin recedes during annealing, and if it is completely annealing out without accompanying slip process, the surface tilt should disappear with the twin, as is the case of small twins less than some

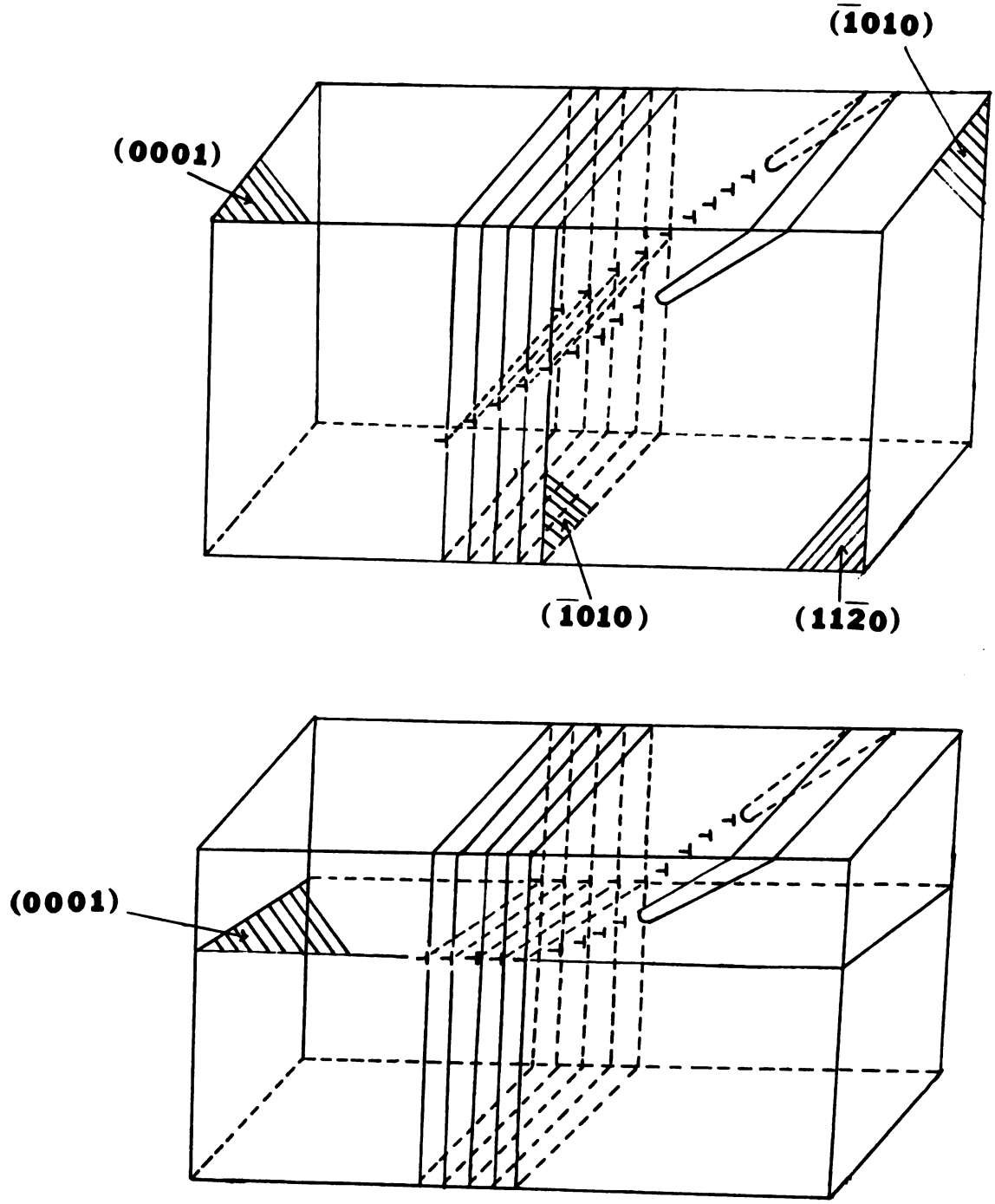

Fig. 37. The polygonization process of the dislocations in the trace left by a receded twin (schematic).
(a) Before annealing.
(b) After annealing.

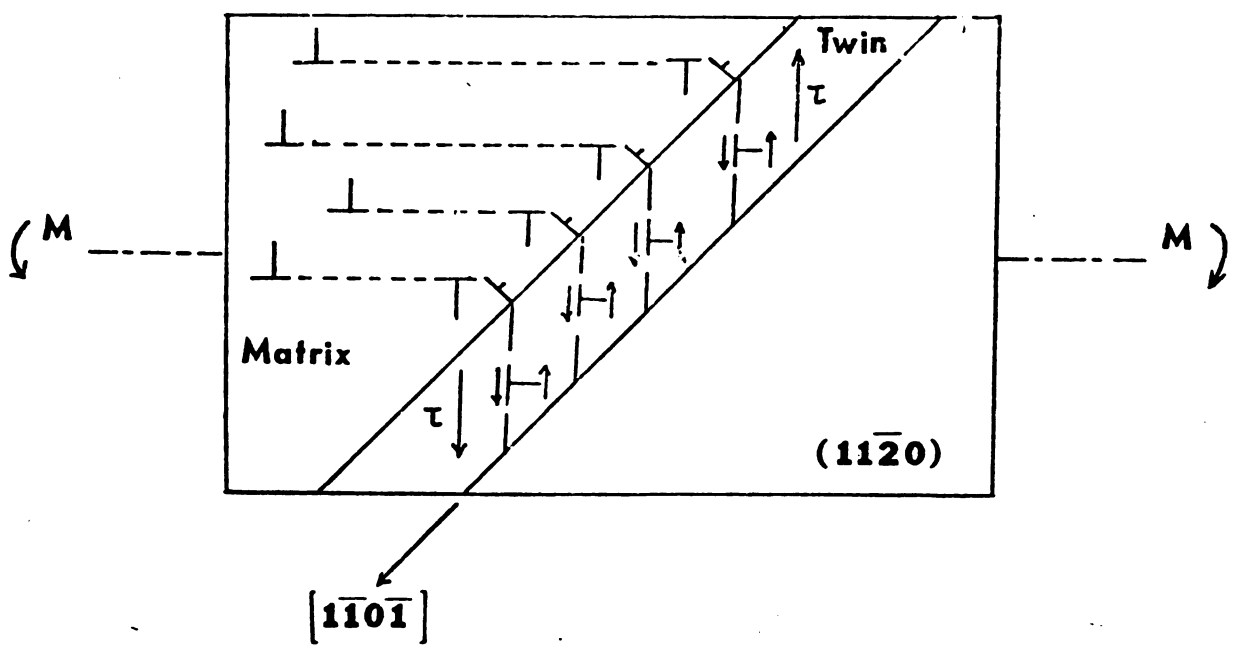

⊥ - - - - ⊤ : Basal dislocation loop in the matrix, $-\vec{a}$ and $\vec{a}$.

: Basal dislocation $-\vec{a}$ in the twin.

⊥ : Dislocation in the matrix along the twin boundary as a result of dislocation incorporation.

Fig. 38. Dislocation reactions along the boundary of a (1$\bar{1}$02)[1$\bar{1}$0$\bar{1}$] twin and the matrix crystal.

1.4μ in thickness. Since such small twins are thermally unstable, therefore recrystallization twins do not exist in cold worked and annealed zinc crystals.

The angle α of the surface tilt associated with the deformation twins, observed previously by other research workers and in the present work, was not always exactly equal to the theoretical value of $3^{\circ}58'$. Since slip in the matrix as well as in the twin usually takes place during twinning, and since slip dislocations if arranged in some specific way such as those in the accommodation kink may give rise to a surface tilt, the surface tilt angle α could be the result of the slip dislocations.

As the twin recedes during annealing, a polygonized wall of twinning dislocations is formed at the tip of the twin. Such a segment of dislocation wall inside the crystal will have a strong stress field around it. In bcc crystals the (112) twin plane is also a secondary slip plane. The high stress field in the neighborhood of such a twin tip may produce the so-called emissary dislocations, which may in turn explain the surface tilt that remains after the twin is completely annealed out. However, in zinc crystals, the $[1\bar{1}02]$ twin plane is not an active slip plane. Emission of dislocations in the twinning plane is not likely to happen. The present work also shows that the dislocations left behind by the receded twin are most likely those slip dislocations resulting from a dislocation incorporation process. To account for the surface tilt that remains after the twin is annealed out, there must be some other dislocation mechanism or mechanisms involved. A possible explanation is that the stress field of the polygonized twinning

dislocations wall may draw neighboring basal slip dislocations with $-\vec{a}$ Burger vector to the twin interface to account for the bend that is opposite to the main accommodation kink.

The final tilt angle that remains after the twin is annealed out would depend on the number of basal dislocations that are drawn to the original twin interface and thus would not be constant. The change in the surface tilt of some 45′ to 50′ as a result of the annealing could be the portion carried away by the disappeared twin not accountable by the slip dislocations drawn to the twin interface. During prolonged annealing, some of the $-\vec{a}$ basal dislocations might combine with the $\vec{c}+\vec{a}$ dislocations to produce the $\vec{c}$ dislocations which polygonize as described previously. A positive proof of the above theory is yet to be found.

4.4 Polygonization of the dislocations in the trace

Fig. 11 shows that the trace which was left behind by the receded twin is bent at the tip after prolonged annealing, and the bent portion of the trace is parallel to the trace of the basal plane. This indicates that the dislocations in the trace have polygonized and formed a boundary perpendicular to the [0001] direction. Since these dislocations were the products of the dislocation incorporation process along the twin boundary, they formed an array parallel to the receded twin boundary before polygonization. This array makes an angle of $46^{\circ}59'$[54,55] with the basal plane of the matrix as shown in Fig. 39.

The array of dislocations is not necessarily in a low energy configuration. Its energy can be lowered by a rearrangement of the dislocations into a low angle boundary that has no long range stress. The

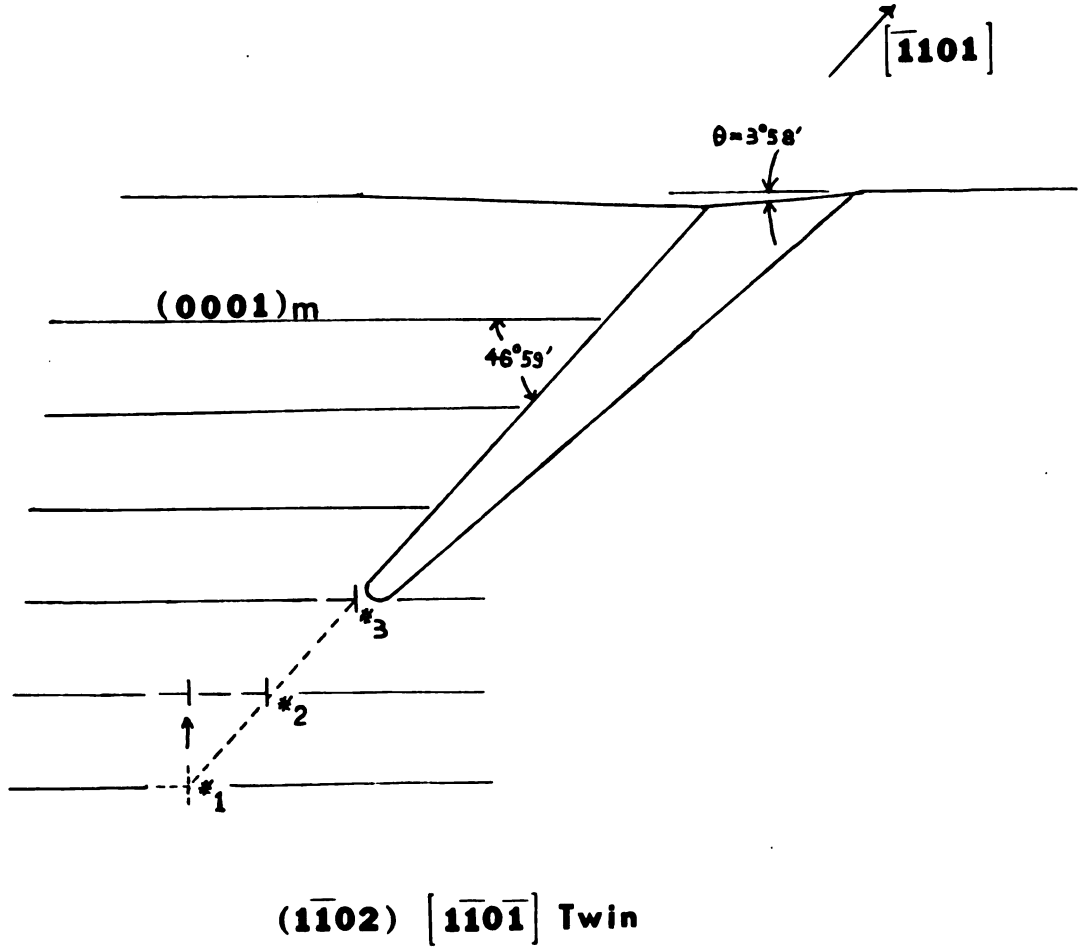

Fig. 39. Polygonization process of the dislocations in the trace (schematic). Plane of the drawing is (11$\bar{2}$0).

forming of this low angle boundary may require dislocation climb and glide, a polygonization process. Thermal activation is needed for the dislocations in the array to polygonize. As shown in Fig. 39, the angle between dislocation #1 and #2 is $46^{\circ}59'$, and hence there is a small repulsion between them. The polygonization is possible only when dislocation #1 can climb into the attractive stress field of dislocation #2. Both dislocations then will move together to dislocation #3. This process continues until the dislocations form a wall. The Peierls-Nabarro force which hinders the movement of the wall will become larger and larger as the height of wall increases, and eventually the movement of the wall will stop. This process is eesentially similar to the polygonization process described in Section 4.1, except for the absence of the twin interfaces. Since the number of dislocations in the trace should be related to the number of slip dislocations in the twin incorporated into the matrix through the twin boundary, the density of the dislocations in the trace would not necessarily be uniform, as was observed to be the case.

During the course of this research, it was found that the polygonization phenomena associated with the dislocations in the trace were related to the loading conditions under which the twins were introduced. When the twins were introduced by the three-point-bending method, prolonged annealing would cause the traces to polygonize readily. But when the twins were introduced by point loading, in most cases the traces did not polygonize. This difference probably lies in the number of $\vec{a}$ dislocations generated in the matrix by the two loading conditions. The three-point-bending method tended to bend the (0001) slip planes of the crystal severely, and hence many basal dislocations with

Burgers vector $\vec{a}$ were generated. On the other hand, the deformation was localized in the point loading method and few basal dislocations were generated. Since $\vec{a}$ dislocations were essential in producing the $\vec{c}$ dislocations in the trace, as described previously, it was reasonable that polygonization of the dislocations in the trace was more likely to occur when the twins were generated by the three-point-bending method. The traces left by the twins which were generated by the point loading method probably consisted of $\vec{c} + \vec{a}$ dislocations that have not combined with basal dislocations to form the $\vec{c}$ dislocation required for the polygonization process.

At the present, one can only say the energy of the polygonized boundary is lower than that of the dislocation array. The detailed process is not exactly known. Further experimental work to clarify this point is needed.

V. CONCLUSIONS

1. Based on a simplified dislocation model, the energy of the coherent twin interface of the $\{1\bar{1}02\}\ \langle 1\bar{1}0\bar{1}\rangle$ twins in zinc crystals has been calculated to lie between 1.4 ± 0.4 and 2.7 ± 0.8 ergs/cm^2.

2. The receding of the tip of such a deformation twin in zinc during annealing has been treated as a polygonization process assisted by the twin interfaces. The theory predicts that when the polygonized wall of twinning dislocations reaches a certain height the process should stop, and the tip of the twin should become parallel-sided.

3. Annealing of zinc single crystals containing deformation twins introduced by either the bending or indentation method at 200°C for ten hours or more shows that those twins whose thickness was less than 1.4×10^{-4} cm would disappear completely with no surface tilt remaining. Those twins with thickness lying between 2 and 35×10^{-4} cm, depending upon the apex angle of the twin, would disappear, but the surface tilt would partially remain. The surface tilts before and after annealing were measured by using an interferometric method and the monochromatic light of the sodium of 589 millimicron in wavelength, and were found to have changed by 45′ to 50′ due to the annealing for those twins of 2 to 35 micron in thickness.

4. By using an etching method suggested by Vreeland et al to bring out the dislocation etch pips, it was confirmed that rows of dislocations were left behind by the receding twin tips after prolonged

annealing. The experimental results also showed that those rows left behind by the twins introduced by bending, polygonized readily to form a dislocation boundary parallel to the basal plane, but those left behind by twins introduced by indentation did not.

5. Attempts were made to identify the character of the rows of dislocation by observing the shape of the etch pips using a scanning electron microscope. The results seem to suggest that the Burgers vectors of the dislocations in the row be $\vec{c} + \vec{a}$, each of which might combine with a neighboring dislocation with a $(-\vec{a})$ Burgers vector to become one with $\vec{c}$, and then polygonize.

6. Since small twins are thermally unstable, annealing twins may not nucleate in zinc crystals.

BIBLIOGRAPHY

BIBLIOGRAPHY

1. Friedel, G., Lecons de Cristallographie, p. 421, Berger Levzault, Paris, 1926.

2. Cahn, R. W., Adv. in Physics, 3, 396, 1954.

3. Mathewson, C. H., Trans. Amer. Inst. Min. Met. Eng., 76, 554, 1928.

4. Mathewson, C. H., and Phillips, A. J., Trans. Amer. Inst. Min. Metall. Engrs., 75, 143, 1927.

5. Krivobok, N. V., Amer. Inst. Met. Eng., Preprint No. 1557-E, 1926.

6. Garber, R. I., Girdin, I. A., Konstantinovskii, M. G., and Startsev, V. I., Doklady Akad. Nauk SSSr 74(2), 343, 1950.

7. Hausner, H. H., and Pinto, N. P., Trans. Amer. Soc. Metals, 43, 1152, 1951.

8. Gindin, I. A., and Startsev, V. I., Zh. EKSper. Teoret. Fiz., 20, 738, 1950.

9. Garber, R. I., Zhur. EKsptl. i Teoret. Fiz., 17(1), 63, 1947B.

10. Cahn, R. W., Adv. in Physics, 3, 363, 1954.

11. Calais, D., Lacombe, P. and Simenel, N., J. Nucl. Materials, 1, 325, 1959.

12. Klassen-Neklyudova, M. V., Mechanical Twinning, Consultants Bureau, New York, p. 72, 1964.

13. Cahn, R. W., Deformation Twinning, p. 8, A.I.M.E. Met. Soc. Conf., Gordon and Breach, New York, 1964.

14. Lavrent'yev, F. F., Soifer, L. M., and Startsev, V. I., Kristallografiya, 5, 3, 472, 1960.

15. Churchman, A. T., J. Inst. Metals, 83, 39, 1955.

16. Lavrent'yev, F. F., and Startsev, V. I., Fiz. Metal. Metalloved, 13, 3, 441, 1962.

17. Rosenbaum, H. S., Acta Met., 9, 742, 1961.

18. Kosevich, V. M., and Bashmakov, V. L., Kristallografica, 4, 749, 1959.

19. Price, P. B., Phil. Mag., 5, 873, 1960.

20. Moore, A. J. W., Acta Met., 3, 163, 1955.

21. Hull, D., Acta Met., 9, 909, 1962.

22. McHargue, C. J., Trans. Met. Soc. AIME, 224, 334, 1962.

23. Hull, D., Deformation Twinning, p. 121, A.I.M.E. Met. Soc. Conf., Gordon and Breach, New York, 1964.

24. Sleeswyk, A. W., Acta Met., 10, 705, 1962.

25. Udin, H., Shaler, A. J., and Wulff, J., Metals Trans., p. 186, 1949.

26. Udin, H., Buttner, F. H., and Wulff, J., J. Metals, p. 1209, 1951.

27. Udin, H., Funk and Wulff, J., J. Metals, p. 1206, 1951.

28. Fullman, R. L., J. of Applied Physics, 22, 4, 448, 1951.

29. Fullman, R. L., J. of Applied Physics, 22, 4, 456, 1951.

30. Mykura, H., Acta Met., 9, 570, 1961.

31. Mykura, H., Acta Met., 9, 595, 1961.

32. Herring, C., The Physics of Powder Metallurgy, McGraw-Hill, p. 143, 1951.

33. Kurdman, J., and Cadek, J., Phil. Mag., 20, 413, 1969.

34. Bhandari, O. P., Bertolott, R. L., and Scott, W. D., Acta Met., 21, 1515, 1973.

35. Nilles, J. L., and Olson, D. L., J. of Applied Physics, 41, 531, 1970.

36. Yoo, M. H., and Wei, C. T., Phil. Mag., 13, 759, 1966a.

37. Murr, L. E., Scripta Met., 6, 203, 1972.

38. McLean, M., and Mykura, H., Phil. Mag., 16, 1191, 1967.

39. Brandt, R. C., Adams, K. H., and Vreeland, T. Jr., J. Appl. Phys., 34, 587, 1963.

40. Chyung, C. K., On the Improvement of Lattice Perfection in High Purity Zinc Crystals Grown from the Melt, M. S. Thesis, Michigan State University, 1962.

41. Jillson, D. S., J. Metals, 188, 1009, 1950.

42. Rais, G. B., Kristallografiya, 3, 325, 1958.

43. Bengus, V. Z., Komnik, S. N., and Startsev, V. I., Doklady Akad. Nauk., SSSR, 141, 607, 1961.

44. Bengus, V. Z., Soviet Physics Crystallography, 8, 322, 1963.

45. Frank, F. C., Phil. Mag., 42, 809, 1951.

46. Bullough, R., Proc. Roy. Soc., A241, 568, 1957.

47. Chyung, C. K., and Wei, C. T., Phil. Mag., 15, 161, 1967.

48. Yoo, M. H., and Wei, C. T., Phil. Mag., 13, 759, 1966a.

49. Eshelby, J. D., Frank, F. C., and Nabarro, F. R. N., Phil. Mag., 42, 351, 1951.

50. Mitchell, T. E., Hecker, S. S., and Smialek, R. L., Phys. State. Sol., 11, 585, 1965.

51. Nabarro, F. R. N., Theory of Crystal Dislocations, p. 75, Oxford Press, 1967.

52. Yoo, M. H., and Wei, C. T., Phil. Mag., 14, 573, 1966b.

53. Gilman, J. J., Trans. Amer. Inst. Min. (Metall.) Engrs., 206, 1326, 1956.

54. Taylor, A., and Leber, Sam., J. of Metals, Feb., 190, 1954.

55. Salkovitz, E. I., Trans. A.I.M.E., 191, 64, 1951.

APPENDICES

APPENDIX A

Polishing and Etching of Dislocations

Present experiment requires polishing and etching solutions which are suitable for undecorated high purity zinc single crystals. It has been found that the solutions developed by Vreeland et al[39] were suitable for the purpose. The solutions are:

P-1		160 gr CrO_3
		20 gr Na_2SO_4
		500 ml distilled water
P-2	Equal parts of:	Methanol
		30% H_2O_2
		conc. HNO_3
P-3		160 gr CrO_3
		500 ml distilled water
E	One part:	1 gr $Hg(NO_3)_2$
		1 ml conc. HNO_3
		500 ml H_2O
	Two parts:	distilled water

The polishing procedure:

1. Dip with mild agitation in solution P-1 for 20-100 sec.
2. Dip occasionally in solution P-2 to accelerate the polishing process.
3. Dip finally in solution P-2 to remove the CrO_3 film.

The etching procedure:

1. Dip with mild agitation in solution E, 5-6 sec.
2. Dip with mild agitation in solution P-1, 5-6 sec.
3. Dip with mild agitation in solution P-3, 2-3 sec.
4. Rinse in running tap water.
5. Rinse in running distilled water.
6. Dry in an air blast.

Best results are obtained when the polishing procedure is immediately followed by the etching procedure.

The formation of etch pips is due to the rapid diffusion of mercury to dislocation sites over the polished surface, and the diffused mercury retards the rate of polishing.

APPENDIX B

Double Beam (Mirau) Interferometer

To measure the surface tilt caused by the twinning process, the Mirau Interferometer was used. This system, contrary to the Multiple Beam Interferometer, is designed to provide for the measurement of surface steps without making contact with the specimen. A light source of low coherence such as a tungsten filament lamp can be used because reference and measuring rays travel exactly the same distance. But to insure accuracy, measurement should be carried out in monochromatic filter or a monochromatic light source. In the present work, a sodium vapor lamp was used as light source.

When the interferometer is tilted against the specimen surface, a fringe system of equidistance fringes is produced. An elevation or depression in the specimen surface causes a displacement of the fringe at this location. The size of this displacement is a direct measure for the height or depth of the steps.

$$d = K\lambda/2 \qquad (1)$$

in which d = step height or depth (μ),

K = relative fringe displacement expressed in parts of one fringe to fringe distance,

λ = used wavelength (589 μ for sodium lamp).

To measure the surface tilt angle θ, as shown in the figure below, eq. (1) can be modified as $d = w/\cot\theta$, in which w is the width of the twin on (0001) surface. Therefore

$$\theta = \cot^{-1} w/d = \cot^{-1} 2w/K\lambda. \qquad (2)$$

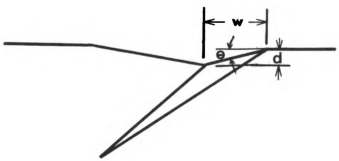

Fig. 40. A twin on $(11\bar{2}0)$ plane (schematic).

APPENDIX C

Equilibrium positions of dislocations in the single-slip-band model

Eshelby et al[49] analyzed the equilibrium positions of n dislocations in a piled-up group under an applied stress. The equilibrium positions $\mathbf{X} = X(i)$ $(i = 1,2,\ldots, n)$ of the dislocations are determined from the equations

$$X(0) = 0$$

$$\sum_{\substack{i=0 \\ i=j}}^{n} \frac{D}{X(j) - X(i)} + \tau = 0 \qquad (j = 1,2,\ldots,n)$$

where $D = \dfrac{Gb}{2\pi(1 - \nu)}$ (isotropic elasticity theory)

$D = \dfrac{Kb}{2\pi}$ (anisotropic elasticity theory)

By considering $X(i)$ as the zeros of the polynomial

$$f(X) = (X - X(1))\,(X - X(2))\ldots(X - X(n)) ,$$

Eshelby et al[49] found that $f(X)$ is given by the first derivative of the n-th Laguerre polynomial

$$f(X) = L_n' \frac{2\tau X}{D} .$$

The equilibrium positions for $n = 1$ to 99 obtained by Mitchell et al[50] are listed in the following Table.

TABLE 1

Equilibrium positions of dislocations in the single-slip-band model.

Equilibrium positions of dislocations in pile-ups are obtained by multiplying by D/2τ.

n	x_1,	x_2,	x_3,	x_4,	x_5,	x_6,	x_7,	x_8	,.....,	x_n
1	2.000									
2	1.268,	4.732								
3	0.935,	3.305,	7.759							
4	0.743,	2.572,	5.731,	10.95						
5	0.617,	2.113,	4.611,	8.399,	14.26					
6	0.527,	1.796,	3.877,	6.919,	11.23,	17.65				
7	0.461,	1.564,	3.352,	5.916,	9.421,	14.19,	21.09			
8	0.409,	1.385,	2.956,	5.182,	8.162,	12.07,	17.25,	24.59		
9	0.368,	1.243,	2.646,	4.617,	7.222,	10.57,	14.84,	20.38,	....,	28.12
10	0.334,	1.128,	2.396,	4.167,	6.487,	9.428,	13.10,	17.70,	....,	31.68
19	0.183,	0.616,	1.301,	2.240,	3.440,	4.911,	6.661,	8.706,	....,	64.65
24	0.146,	0.493,	1.039,	1.786,	2.738,	3.893,	5.273,	6.868,	....,	83.37
29	0.122,	0.410,	0.864,	1.485,	2.275,	3.236,	4.370,	5.682,	....,	102.3
39	0.091,	0.307,	0.647,	1.112,	1.702,	2.417,	3.260,	4.231,	....,	140.4
49	0.073,	0.246,	0.517,	0.888,	1.359,	1.930,	2.601,	3.374	,....,	178.8
59	0.061,	0.205,	0.431,	0.740,	1.132,	1.607,	2.165,	2.807,	....,	217.4
69	0.052,	0.175,	0.369,	0.634,	0.970,	1.376,	1.854,	2.403,	....,	256.1
79	0.045,	0.153,	0.323,	0.555,	0.848,	1.204,	1.622,	2.101,	....,	295.0
89	0.040,	0.136,	0.287,	0.493,	0.754,	1.070,	1.441,	1.867,	....,	334.0
99	0.036,	0.123,	0.258,	0.444,	0.678,	0.962,	1.296,	1.680,	....,	373.0